In situ $\delta^{13}C$ and $\delta^{18}O$ microanalysis by SIMS: A method for characterizing the carbonate components of natural and engineered CO_2-reservoirs

Maciej G. ŚLIWIŃSKI[1*], Kouki KITAJIMA[1], Reinhard KOZDON[1,2], Michael J. SPICUZZA, Adam DENNY[1] and John W. VALLEY[1]

[1] *WiscSIMS, Department of Geoscience, University of Wisconsin-Madison, Madison, WI, 53706*
*Corresponding author: msliwinski@wisc.edu

[2] *Lamont-Doherty Earth Observatory of Columbia University, Palisades, NY, 10964*

Abstract

This work addresses the potential utility of *in situ* carbon and oxygen isotope microanalysis ($\delta^{13}C$ and $\delta^{18}O$) by *secondary ion mass spectrometry* (SIMS) in carbon sequestration research. A desirable long-term consequence of CO_2-injection into underground rock formations at prospective sequestration sites (such as deep saline sandstone aquifers capped by impermeable strata) is the precipitation of carbonate mineral cements, the isotopic fingerprinting of which is a central theme here. More specifically, we focus on the unique advantage of the SIMS technique, which lies in the capability of analyzing very small sample volumes that are otherwise inaccessible to sampling techniques in conventional *isotope ratio mass spectrometry* (IRMS). For example, single carbonate crystallites as small as 3-10 µm across can be readily analyzed by SIMS with sub per-mil (‰) accuracy and precision. Importantly, the ability to perform micrometer-scale measurements *in situ* from either thin sections or 1-inch (25 mm) diameter polished core plugs preserves the petrographic context of measured carbonate $\delta^{18}O$ and $\delta^{13}C$ values.

We provide a preliminary characterization of the pre-injection mineralogy and isotopic fingerprints of carbonate cements in the Mount Simon Sandstone reservoir and the overlying shaly caprock (the Eau Claire Formation) at the Illinois Basin Decatur Project, a demonstration and research site for exploring the feasibility of long-term CO_2 storage in a deep saline aquifer. By drawing upon published data on ambient reservoir conditions and the isotopic composition of the injected CO_2, we make simple predictions regarding possible $\delta^{13}C$ values of calcite, dolomite-ankerite, and siderite cements that may form in response to long-term CO_2 storage.

Key words: carbon sequestration, natural analogues, carbonate cements, carbon isotopes, SIMS microanalysis, Illinois Basin, Illinois Basin Decatur Project

Introduction

Geological storage of carbon dioxide gas (CO_2) emissions produced by human industrial and agricultural activities is actively being evaluated as a means of mitigating global climate change (*e.g.,* Bachu et al., 1994; Celia et al., 2015; DePaolo and Cole, 2013; DOE, 2010; IPCC, 2005; Lackner et al., 1995; Matter et al., 2016; Power et al., 2013). Capturing CO_2 from stationary point sources (*e.g.,* coal-fired power plants) and storing it in geological environments, such as in deep saline aquifers, is a technologically feasible (*e.g.,* Hosa et al., 2011; Michael et al., 2010, 2009) and potentially viable stand-in solution for some time to come as societies gradually transition to alternative, and more sustainable, clean energy-producing technologies (*e.g.,* Baines and Worden, 2004a; Bickle, 2009; Celia et al., 2015; Gale, 2004; Hoffert et al., 2002; Lackner, 2003). At present, the large-scale deployment and implementation of this carbon capture and storage (CCS) strategy is seemingly impeded first and foremost by economic inconvenience (*e.g.,* Celia et al., 2015; Gibbins and Chalmers, 2008; Michael et al., 2009; Orr, 2009; Wigley et al., 1996).

An important objective of research efforts concerned with the feasibility of sequestering carbon in a variety of potentially suitable geological environments (*e.g.,* deep saline sandstone aquifers, depleted oil and gas reservoirs, unmineable coal seams, flood basalt provinces or ultramafic rock formations; Baines and Worden, 2004a; McGrail et al., 2006) is the ability to make realistic predictions about the long-term fate of stored CO_2 (on a time scale exceeding 10,000 years). A recent volume of Reviews in Mineralogy and Geochemistry showcases some of the modern techniques and approaches that are being applied in this field of research (DePaolo and Cole, 2013) and outlines the leading geologically-oriented thematic questions; among others,

these include the following: What is the relative importance of different CO_2-trapping mechanisms in different types of prospective reservoirs, and how long are they effective (*e.g.,* structural/stratigraphic or solubility trapping vs. carbon mineralization; Gunter et al., 2004)? What geochemical reactions are likely to occur (and at what rates) between the waters/brines in geological formations that become reactive due to CO_2-charging and the specific mineralogy of a given reservoir-caprock system? What is the capacity for reactions to consume CO_2 and produce carbonate mineral cements, where in the system will such cements form, and over what time scales are such reactions likely to occur? This process, referred to as carbon mineralization (or mineral trapping), is the most secure and effectively permanent form of long-term CO_2 storage.

Much insight into many of the above questions concerning the long-term fate of sequestered CO_2 comes from studies of so called natural analogues, or geological environments where large quantities of CO_2 have accumulated and remained confined over geologic time scales (*e.g.,* Baines and Worden, 2004b; Bickle et al., 2013). Such accumulations exist, for example, in certain deeply-buried permeable sandstone formations (saline aquifers/reservoirs) that are overlain by effectively impermeable sediments that act as seals (or 'caprocks', *e.g.,* shales or salt beds; Haszeldine et al., 2005; Heinemann et al., 2013; Lu et al., 2011, 2009; Pearce et al., 1996; Sathaye et al., 2014; Watson et al., 2004; Wilkinson et al., 2009). For a given reservoir-caprock system, studies of natural analogues help to characterize the predominant fluid-mineral reactions that could be reasonably expected during engineered CO_2 storage and allow for estimating rates of carbon mineralization. They further provide a means of ground-truthing (or 'history-matching') the results of geochemical models that seek to predict how a particular type of reservoir will evolve in the long-term as its mineralogy is subjected to a CO_2 charge. In this regard, the knowledge gained from natural analogues is indispensable for the simple reason that

rates of geochemical reactions are generally not well constrained at the relatively low temperature conditions of many prospective CO_2 storage reservoirs, which severely limits the predictive power of models. Gaines and Worden (2004b) make an elegant point in noting that a model generally "tells us how a rock [or given reservoir unit] should evolve to reach thermodynamic equilibrium, not whether it will evolve," and does not "inform us how long (or even if) a reaction will occur."

With regards to estimating rates of carbon mineralization in a given reservoir-caprock system, a substantial difficulty in natural analogue studies commonly lies in distinguishing carbonate cements that precipitated as an eventual consequence of natural CO_2-charging from those cements that may have formed during earlier stages of sediment alteration (Heinemann et al., 2013; Wilkinson et al., 2009). In the case of sandstone reservoirs, the presence of earlier-formed carbonates would not be unusual as carbonate minerals are a predominant cement type in such rocks types (Morad, 2009). Measurements of stable isotope ratios of carbon and oxygen ($\delta^{13}C$ and $\delta^{18}O$, respectively) can serve as a useful diagnostic tool; however, drawing distinctions based on the results of conventional sampling techniques (or step-wise acid-digestion procedures) can be complicated because a thorough mechanical separation of different carbonate cement populations is often not possible due to small crystal size (or steep compositional gradients in larger crystals).

This study aims to demonstrate the applicability in carbon sequestration research of recent advances in the analytical methods of measuring carbon and oxygen isotope ratios in carbonate minerals by secondary ion mass spectrometry (SIMS). This technique allows for micrometer-scale measurements to be made *in situ* from either thin sections or 1-inch diameter core plugs, thus preserving the petrographic context of analyzed sample volumes (*e.g.,* Śliwiński

et al., 2015a, 2015b; Valley and Kita, 2009). To this end, we provide a preliminary characterization of the mineralogy and the isotopic fingerprints of the major existing carbonate cement generations in the upper Mt. Simon Sandstone reservoir and the overlying Eau Claire shale at the Illinois Basin Decatur Project site (IBDP; Fig. 1), where 1 million metric tons of CO_2 have now been successfully injected to demonstrate the technological feasibility of sequestration in a deep saline sandstone reservoir (DOE, 2010; Leetaru et al., 2009; Leetaru and Freiburg, 2014). The technique we describe may more broadly find use as a tool for monitoring the progress of carbonate mineral cement-forming reactions within reservoir-caprock systems, especially during the early post-injection period (years to decades?), when only small volumes of new carbonate will likely be forming. As little as 3 micrometers (μm) of new cement growth could be readily analyzed by SIMS with sub-per mil accuracy and precision, and such data could conceivably be the basis for quantitative, up-scaled reservoir simulations that attempt to predict the eventual volume of CO_2 that may become securely trapped in mineral form. Smaller, nanometer-scale domains can be analyzed using a sub-μm spot (Page et al., 2007) for systems where compositional contrasts are greater.

2. Methods

The sandstone beds examined in this study were collected from the transition zone between the upper unit of the Upper Cambrian Mt. Simon Sandstone and the basal unit of the overlying Eau Claire Fm. from core material recovered from the IBDP Verification Well #1 (Fig. 1), at depths of 1680.4 m (5513.2 ft), 1677.3 m (5502.9 ft), and 1676.8 m (5501.3 ft) (this depth interval corresponds to Unit A of Palkovic (2015) - see Fig. 4.1 therein). Due to sampling restrictions, the overlying Eau Claire Fm. was sampled from core material from a well in a

nearby county, ~75 km (~45 miles) to the WSW of IBDP (C13637, at a depths of 1096.5 m (3597.5 ft), 1096.7 m (3598 ft) and 1094.8 m (3592 ft); Fig. 1).

Subsamples of core (Fig. 2) were first roughly polished using a series of diamond-embedded abrasive pads (20, 10 and 6-µm) and examined by scanning electron microscopy (SEM; Hitachi S3400-N) to quickly and efficiently locate carbonate-cemented intervals. For this initial examination, the sample surfaces were not coated with a conductive material (*e.g.,* with carbon, Au, Ir, etc.) as is customary for high-resolution imaging, and the SEM was instead operated in variable-pressure mode to reduce the detrimental effects of charging on image quality. Carbonate cements were identified using energy-dispersive x-ray fluorescence spectroscopy (ED-XRF; ThermoFisher detector coupled to SEM).

A further sub-sample (*ca.* 1 cm^3) was taken from well-cemented intervals and cast into 25-mm diameter epoxy mount (Mt. Simon sampled at 1680.4m / 5513.2 ft (see Fig. 2c), Eau Claire at 1096.5 m / 3597.5 ft). As is standard practice at the WiscSIMS laboratory, several grains of microanalytical reference materials (RMs) were embedded in the center of each mount for the purposes of monitoring instrumental drift and for correcting sample matrix effects during subsequent isotope ratio analyses by SIMS. The following RMs were used: dolomite "UW6220" ($\delta^{18}O$ = 22.60‰ relative to Vienna Mean Standard Ocean Water (VSMOW), $\delta^{13}C$ = 0.84‰ relative to the Vienna PeeDee Belemnite standard (VPDB); Śliwiński et al., 2015a,b) and quartz "UWQ-1" ($\delta^{18}O$ = 12.33‰ VSMOW; Kelly et al., 2007). The mount was then polished to a 0.25-µm finish, cleaned with ethanol and deionized water, and lastly coated with a thin layer of gold (25 nm thickness) to make the sample surface electrically conductive for subsequent $\delta^{13}C$ and $\delta^{18}O$ analyses by SIMS. The gold coat was later removed and replaced with a coat of carbon

(25 nm thickness) for electron probe microanalysis (EPMA) to determine the chemical composition of different carbonate cement zones.

Samples were examined petrographically by means of high-resolution back-scattered electron (BSE) and cathodoluminescence (CL, Gatan PanaCL) SEM imaging; in the case of the Mt. Simon Sandstone sample, CL-imaging of quartz cements (quartz-overgrowths) was essential to establishing the relative order of major stages in the quartz and carbonate cementation histories (SA 1). CL-imaging of quartz cements was performed with the sample very thinly coated with carbon (~5 nm) to maximize the signal strength; no filters were employed. We found that many of the CL-features visible in the images of quartz cements that follow were either heavily subdued or not discernable altogether with a standard thickness carbon coat (25 nm).

We provide here an abridged account of the SIMS methodology. The interested reader is referred to Śliwiński et al. (2015a,b, 2016) for further details. *In situ* carbon and oxygen isotope ratio measurements were performed using a CAMECA IMS 1280 large radius multicollector ion microprobe (Department of Geoscience, University of Wisconsin-Madison). Measured isotope ratios are reported using conventional δ-notation, which expresses the per mil (‰) deviation of a measured ratio from an internationally accepted reference value (VSMOW for $\delta^{18}O$ and VPDB for $\delta^{13}C$ analyses).

The analytical precision of SIMS $\delta^{18}O$ measurements at WiscSIMS is typically ± 0.3‰ (2SD, standard deviations) for a sample spot-size of 10 micrometers and ± 0.7‰ (2SD) for 3-micrometer spots; this follows from the spot-to-spot repeatability of replicate measurements (n = 8) of a running standard (or drift monitoring material, in this case dolomite "UW6220") which bracket each set of about 10 sample analyses. For $\delta^{13}C$ measurements employing a 6-micrometer spot-size, the typical precision is 0.6-1.2‰ (2SD).

171 The analytical accuracy of SIMS $\delta^{18}O$ and $\delta^{13}C$ measurements is affected by instrumental
172 mass fractionation and sample matrix effects (collectively referred to as the 'bias'; *e.g.,* Eiler et
173 al., 1997; Hervig et al., 1992; Kita et al., 2009; Valley and Kita, 2009). This bias is a measure of
174 the per mil (‰) difference between measured 'raw' and 'true' (*i.e.,* VPDB or VSMOW) values of
175 $\delta^{13}C$ or $\delta^{18}O$. For a given configuration of the secondary ion mass spectrometer, the influence of
176 instrumental parameters to total bias during an analytical session can be held nearly constant; any
177 instrumental drift that occurs can be monitored and corrected by regularly analyzing a running
178 standard (or drift-monitoring material). For minerals that exhibit solid-solution behavior, this
179 leaves the component of total bias that is a function of variable chemical composition (*i.e.,* the
180 sample matrix effect) in need of calibrating. The development of reference materials along with
181 calibration schemes for the analysis of carbonate mineral compositions that fall along the
182 dolomite-ankerite solid solution series was previously reported by Śliwiński et al. (2015a,b).
183 These bias corrections require that the chemical composition in the immediate vicinity of each
184 SIMS pit be known with a high degree of precision, especially in the case of low-Fe dolomites
185 (up to several wt.% Fe). To correct the data presented here, chemical analyses were performed
186 by EPMA (using a CAMECA SX-51 at the Cameron Electron Microprobe Laboratory,
187 Department of Geoscience, University of Wisconsin-Madison).
188 The accuracy of sample analyses is determined in large part by the residuals of the SIMS
189 $\delta^{18}O$ and $\delta^{13}C$ calibration curves for carbonates of dolomite-ankerite series. The residuals reflect
190 how well the bias correction scheme for each isotope system reproduces data for a suite of 13
191 reference materials in relation to the certified reference material NBS-19. For O-isotope analyses
192 employing a 10-µm diameter spot-size and C-isotope analyses employing a 6-µm spot-size, the
193 residual is typically constrained to ± 0.3‰ (2SD). The residual increases slightly to ± 0.4‰

194 (2SD) when analyzing O-isotope ratios using a 3-µm diameter spot-size Śliwiński et al.
195 (2015a,b).
196
197 **3. Results**
198 ***3.1. Chemical zoning patterns in carbonate cements***
199 On the basis of BSE imaging by SEM - a mode that is sensitive to variations in chemical
200 composition - we identified six major stages of carbonate (dolomite-ankerite) cementation within
201 the examined sandstone bed of the upper Mt. Simon Fm. Each successive stage appears as a
202 concentric zone with a distinct 'BSE texture' and sharp compositional boundaries with the
203 preceding and/or succeeding cement zones (Fig. 3b; SA 1). Texturally, zones 4-6 are
204 predominately characterized by layering/banding; this is evidenced by subtle, concentric, within-
205 zone variations in the shades of gray seen in BSE images (indicative of changes in chemical
206 composition that are more subtle within zones than they are among zones). In contrast, the
207 texture of zones 1-3 can be described as 'mottled' and suggests some degree of recrystallization
208 (*sensu* Machel, 1997). The carbonate cement morphology takes the form of poikilotopic crystals
209 measuring up to ~500 µm across, with well-developed crystal faces where pore space permits
210 (Fig. 3b, SA 1).
211 Carbonate cement zones were classified in terms of chemical composition/mineralogy
212 according to the scheme of Chang et al. (1998), where the dolomite-ankerite solid-solution series
213 is sub-divided on the basis of Fe-content as follows: 1) non-ferroan dolomite (NFD; Fe#: 0.0-0.1,
214 where Fe# = molar Fe/(Mg+Fe), equivalent to 0-5 mole% Fe (*i.e.* Fe/(Ca+Mg+Fe)), 2) ferroan
215 dolomite (FD; Fe#: 0.1-0.2, equivalent to 5-10 mole% Fe), and 3) ankerite (Ank; Fe# > 0.2,
216 equivalent to >10 mole% Fe). Accordingly, zones 1 and 2 straddle the boundary between ferroan

dolomite and ankerite; zone 3 is a low-Fe ankerite (Fe#: 0.20-0.25); zone 4 is a ferroan dolomite; and zones 5 and 6 are distinctly Fe-rich ankerites (Fe#'s extending to 0.5; Fig. 4a-b, Table 1).

Six major stages of carbonate (dolomite-ankerite) cementation were also identified within the examined Eau Claire shale sample (Figs. 3a, 5), although we cannot establish how these correlate to the cement zones in the Mt. Simon Sandstone. The cement morphology is dominated by euhedral crystals, typically measuring < 100 μm across. The chemical zoning pattern is concentric, with no major dissolution features or mottled textures that would suggests some degree of recrystallization (Figs. 3a, 5). An abrupt change in composition is noted between: zones 0 (NFD) and 1a (FD-Ank); zones 1b (FD) and 2a (Ank); and again between zones 2b (Ank) and 3 (NFD) (Figs. 5 and 6a-b). In contrast, the change in composition is more gradational between zones 1a (Ank-FD) and 1b (FD) and again between zones 2a and 2b; nonetheless, two distinct sub-domains are evident in both instances in BSE-imagery: a relatively Fe-rich inner domain (zones 1a and 2a) and a less Fe-rich outer domain (zones 1b and 2b; Figs. 5 and 6a-b).

3.2. Trends in the isotopic composition ($\delta^{13}C$ and $\delta^{18}O$) of carbonate cements

The results of *in situ* SIMS $\delta^{13}C$ and $\delta^{18}O$ analyses are summarized in Tables 1 and 2 and are presented graphically in Figs. 3-6. Throughout this article, values of $\delta^{13}C$ are expressed relative to the VPDB standard, whereas those of $\delta^{18}O$ are expressed relative to VSMOW; for convenience, $\delta^{18}O$ values are also tabulated relative to VPDB in Tables 1 and 2. The complete dataset, which includes all measured signals (*e.g.* count rates, backgrounds, counting statistical errors, etc.) from reference materials and analyzed sample regions, as well as the calibration model parameters used to correct for sample matrix effects, is provided in Supplementary Appendices 2-4. Supporting petrographic documentation, which includes individually-annotated

240 SIMS pits, is provided as a SA 1. Patches of carbonate cement in multiple sample sub-domains
241 were analyzed to ensure that measured values are representative ('sample regions' in Tables 1 and
242 2 and SA 1).

243 Two distinct data clouds are apparent in cross-plotting $\delta^{13}C$ vs $\delta^{18}O$ (Fig. 3c); one is
244 populated by sample data from the upper Mt. Simon sandstone beds, and is generally
245 characterized by increasingly negative $\delta^{13}C$ values that extend from +1 to -9‰ (VPDB) (to a
246 first-order across zones 0 through 6). The other data cloud represents the overlying silty-shaly
247 Eau Claire Fm. and stands in stark contrast, being characterized by positive $\delta^{13}C$ values that
248 extend from +2 to +16‰ (VPDB) (to a first-order across zone 0 through 3). Given the small
249 sample subset at this stage of research, however, it is too early to generalize about differences on
250 a formation-wide scale. Please note that based on conventional isotope analyses performed on a
251 larger suite of bulk samples, it is known that carbonate $\delta^{13}C$ variability exists among the four Eau
252 Claire sub-units at the IBDP site (Palkovic, 2015). To a first-order, differences in bulk $\delta^{13}C$
253 values – extending from approx. -4‰ to +4‰ VPDB up through the section – correlate to
254 changes in lithology, although depth-dependent changes within individual sub-units are also
255 evident (most clearly seen in the top-most Unit D; refer to Fig. 5.8 in Palkovic, 2015). Additional
256 *in situ* characterizations of lower Eau Claire carbonate cements from across the Illinois Basin are
257 reported elsewhere (Śliwiński et al., 2015c, 2016). What we in-part attempt to demonstrate here
258 is the ability to retrieve another layer of information by interrogating isotopic records on a finer
259 spatial scale. Some potential applications where this may be useful in relation to carbon-
260 sequestration research are discussed later on.

261 A moderate linear correlation is apparent in the cross-plot of carbonate $\delta^{13}C$ and $\delta^{18}O$
262 values measured from the Mt. Simon Sandstone (adjusted $R^2 = 0.61$; Fig. 3c). To a first-order,

263 $\delta^{18}O$ values progressively decrease across early-to-late cement generations from a high of ~22‰
264 VSMOW (zone 1) to a low of ~16‰ (zone 6) (Figs. 3d and 4c). Notably, however, carbonate
265 $\delta^{18}O$ values measured from zone 4 abruptly break this trend and transiently increase to a high of
266 ~24‰ (values also increase throughout this stage of cement development from ~20 to 24‰; SA
267 1). The corresponding carbonate $\delta^{13}C$ values measured from zones 1-3 fall within the relatively
268 narrow range between 0 and -3‰ (VPDB), and then systematically decrease down to -9‰ across
269 zones 4-6 (Fig. 4d; SA 1).

270 Carbonate $\delta^{13}C$ and $\delta^{18}O$ values measured from different cement generations of the Eau
271 Claire shale show no correlation (Fig. 3c). Nonetheless, carbonate $\delta^{18}O$ values progressively
272 decrease across early-to-late cement generations from a high of ~26‰ (zone 0) to a low of
273 ~22‰ (zone 3) (Fig. 6c). It is notable that, on average, $\delta^{18}O$ values measured from the shale bed
274 cements are ~4‰ higher than those in the underlying sandstone (same first-order decreasing
275 trend with a ~4‰ offset; compare Figs. 4c and 6c). The $\delta^{13}C$ values of the earliest stage of
276 cement development (zone 0) fall between 3-4‰ (VPDB) and, in stark contrast to the sandstone
277 beds, increase abruptly during subsequent stages of cement growth; values span the range
278 between +7 and +15‰ across zones 1a and 1b, but fall somewhat to between +6 and +11‰
279 across zones 2a, 2b, and 3 (Fig. 6d).

280

281 ***3.2. Trends in the isotopic composition ($\delta^{18}O$) of quartz cement in the upper Mt. Simon***
282 ***Sandstone***

283 On the basis of CL-imaging, we identified four major stages of quartz cementation (QO
284 1-4) within the examined sandstone bed of the upper Mt. Simon Fm. (Fig. 7; SA 1). Detrital
285 quartz grains are indistinguishable from their respective quartz overgrowths (cement) by BSE-

286 imaging. However, this distinction can be readily made by employing a CL-detector coupled to
287 an SEM, which allows for observing layering/banding (if present) within individual overgrowths
288 (indicative of different cementation stages) (Fig. 7).

289 Quartz cement deposited during stages 1-3 is CL-luminescent, whereas quartz cement
290 formed during the final stage is characteristically non-luminescent and qualitatively constitutes
291 approx. one-half of the total cement volume (Fig. 7). In terms of $\delta^{18}O$ values, quartz cement
292 zones 1, 2 and 3 fall between 24‰ and 21‰, and a mild tendency towards lower values is
293 observed with each successive cement generation (Fig. 4e). Quartz cement zone 2 is conspicuous
294 in that $\delta^{18}O$ values abruptly break the trend defined by zones 1, 3 and 4 by transiently increasing
295 to ~27.5‰ (Fig. 4e). For additional information on $\delta^{18}O$ zoning in quartz-overgrowths of the Mt.
296 Simon Sandstone within the Illinois Basin, the interested reader is referred to the work of
297 Pollington et al. (2011). No quartz-overgrowths were analyzed from the Eau Claire shale in the
298 course of this study, but were previously examined by Hyodo et al. (2014).

299

300 ***3.3. Microstratigraphic relationships among cements (upper Mt. Simon Sandstone)***

301 With regards to the microstratigraphic relationships among individual quartz-overgrowth
302 and carbonate cements zones, we have observed the following (refer also to SA 1):

303

304 1) Based on an image analysis, dolomite-ankerite cement zones 1-4 comprise approx. 75% of the
305 total carbonate cement volume (using ImageJ; Schneider et al., 2012). These four generations of
306 cement precipitated *before* the onset of quartz cementation (Figs. 4f and 7; SA 1). Dolomite-
307 ankerite zones 1-4 developed atop detrital quartz grain boundaries, which were free of any
308 quartz-overgrowths at this stage of sediment lithification. Do note, however, that a portion of

detrital quartz grains have partially corroded/embayed grain boundaries (see petrographic documentation in SA 1); in sample regions where this is evident, carbonate cements appear to locally replace quartz, but only to a limited extent (Burley and Kantorowicz, 1986a, 1986b). This type of texture predominates where detrital quartz grains are in contact with dolomite-ankerite cement zones 1-3, which, based on their mottled texture, appear to have recrystallized (Machel, 1997). Quartz-overgrowths are optically continuous with detrital cores, non-fibrous, and appear pristine. Where present, the underlying detrital quartz grain boundaries show no corroded textures.

2) The development of quartz-overgrowth zones 1 and 2 largely overlapped in time with the formation of carbonate cement zone 5 (Fig. 4f). However, a portion of carbonate cement zone 5 was already in place at the onset of QO zone 1 growth; this stage of carbonate cementation also continued for some time after QO zone 2 fully developed.

3) The development of quartz-overgrowth zones 3 and 4 largely overlapped in time with the development of carbonate cement zone 6 (Fig. 4f). However, a portion of QO zone 3 was already in place as carbonate cement zone 6 began forming, and this stage of carbonate cementation continued for some time after the end of QO zone 4 growth.

4. DISCUSSION (Parts I and II)

The focus of the discussion that follows is two-fold: Part I is concerned with the IBDP site and simple predictions regarding possible $\delta^{13}C$ values for carbonate cements that are expected to form in response to long-term CO_2 storage. In Part II, we identify potential

applications where carbonate isotope microanalysis by SIMS could contribute uniquely to research efforts concerned with geologic carbon storage. In keeping with the largely methodological theme of this article, a brief discussion on the evolution of isotope ratios in cements that formed during sediment burial and alteration at/near the IBDP site is provided as a supplemental discussion (SA 5).

PART I: Relevance to the Illinois Basin Decatur Project

Distinguishing carbonate mineral cements that form in response to CO_2 injection at the IBDP site from those that have formed naturally in response to prior, burial-related alteration of the sediment (diagenesis) would entail establishing a pre-injection petrographic baseline (one larger in scope than the small number of samples examined here) for the relevant carbonate-cemented intervals of the reservoir and basal caprock units. Such a baseline could be strongly reinforced by chemical and isotopic fingerprinting ($\delta^{13}C$ and $\delta^{18}O$). However, only small volumes of new carbonate are likely to form in the initial post-injection years, and so it may difficult to perform isotopic fingerprinting by conventional techniques, especially in the likely scenario where mechanical separation of new and preexisting cements will not be feasible. *In situ* isotope microanalysis by the SIMS technique offers a way past these technical obstacles.

Volumetrically significant occurrences of carbonate cement (predominantly dolomite-ankerite) locally occupy the pore space of the upper Mt. Simon Sandstone, nearby/within the gradational contact (Leetaru and Freiburg, 2014) with the overlying shaly Eau Claire Fm. (Bowen et al., 2011; Fishman, 1997; Hoholick et al., 1984). Although somewhat limited in scope, our petrographic survey has additionally identified the presence of Mg-siderite cements in the upper Mt. Simon in samples from the basin margin in northern Illinois (relatively shallow

355 burial environment; max. burial ≈ 1 km / 3,500 ft; after Rowan et al., 2002) and at depth in the
356 southern Illinois Basin (max burial ≈ 5.5 km / 18,000 ft; Figs. 1 and SA 1, Plate 24). While we
357 did not observe such cements at the intermediate burial depths of this unit at the IBDP site, they
358 have been documented in IBDP wells (*e.g.,* Palkovic, 2015). Limited analyses indicate that
359 carbonate minerals (calcite, dolomite) are also present in mudstone/shale interbeds at depth in the
360 general vicinity of the CO_2 injection zone within the lower Mt. Simon Sandstone (*e.g.,* see Table
361 8.3 in Finley, 2005). These clay mineral-rich interbeds are considered to be the first reactive
362 environments that will be encountered by the emplaced CO_2 plume as it buoyantly rises through
363 the reservoir, and are estimated to have the same capacity for sequestrating carbon by mineral-
364 trapping reactions as the basal Eau Claire shale (Finley, 2005). Isotopic fingerprinting could aid
365 comparative studies of cements from these intervals in core material recovered at IBDP prior to
366 injection (2011-2014) and in sample material that may be recovered at some future time in the
367 post-injection/monitoring phase currently underway. Such studies could aid in ground-truthing
368 and/or refining reactive flow and transport models that attempt to: 1) predict the rate of mineral-
369 trapping reactions, 2) to delimit the likely spatial distribution of reaction products (carbonate
370 cements), and 3) to estimate the amount of CO_2 that will likely become permanently
371 immobilized in mineral form (*e.g.,* Liu et al., 2011). Note that whereas the injection zone is
372 situated within the lower Mt. Simon Fm at the IBDP site, injection was also planned into the
373 upper portion of this reservoir unit at the nearby site of the FutureGen 2.0 project (now
374 defunded; *e.g.,* Bonneville et al., 2013; Vermeul et al., 2016).

375 Within the diverse suite of lithofacies that comprise the Eau Claire shale, carbonate
376 cements are generally abundant, although somewhat heterogeneously distributed (*e.g.,* Finley,
377 2005; Neufelder et al., 2012; Palkovic, 2015; Śliwiński et al., 2016). Carbon mineralization

reactions are especially anticipated to occur along the reservoir-caprock interface where reactive Fe-rich clay minerals and carbonate cements occur in abundance (Finley, 2005). Limited natural analogue studies indicate that chemical reactions between CO_2 and the caprock mineralogy can extend across a thickness of 10+ meters of the basal caprock layer (Bickle, 2009; Lu et al., 2009). During the initial post-injection pH buffering stage, carbonate cements in this basal layer may undergo partial to complete dissolution and subsequently re-precipitate higher within the unit (*e.g.,* Kaldi et al., 2011). The depth of CO_2 penetration/reaction can generally be traced by means of $\delta^{13}C$ analysis (*e.g.,* Lu et al., 2009), although the very small size of cement crystals in mudrocks/shales can complicate attempts at obtaining end-member signals from different carbonate components by means of conventional sampling/analytical techniques (*e.g.,* Heinemann et al., 2013; Wilkinson et al., 2009).

A limited number of recent laboratory-scale experimental studies have investigated the reactivity of the IBDP reservoir and caprock units under simulated CO_2 storage conditions. Discernable changes in rock texture and mineralogy were noted within only a years' time, and indicate a tendency for dissolution of clay minerals that line the pore throats of the Mt. Simon Sandstone and for corrosion/degradation of illite, chlorite, K-feldspar, biotite and pyrite in the Eau Claire shale (Yoksoulian et al., 2013). Iron-bearing clays were identified as a key reactant at IBDP, and are expected to help contribute the aqueous cations (Fe^{2+}, Mg^{2+}) necessary for carbon mineralization (Carroll et al., 2013; see also, *e.g.,* Alemu et al., 2011; Kaldi et al., 2011). Reactive transport model simulations estimate that at least 10 to 20% of the introduced CO_2 may eventually be consumed in the precipitation of Fe-bearing carbonate cements (Liu et al., 2011), although this estimate would likely increase if the reactivity of Fe-rich clays with CO_2-charged brine were taken into consideration (Carroll et al., 2013).

401

402 **4.1 Forecasting $\delta^{13}C$ values for sequestration-related carbonates at IBDP**

403 Here we make use of available data on reservoir conditions and the C-isotope ratio of the
404 injected CO_2 at the IBDP site (*e.g.,* Finley, 2005) to make simple predictions about the possible
405 isotopic fingerprints of different carbonate cement types (*e.g.,* calcite, dolomite-ankerite,
406 siderite) that may form in response to long-term CO_2 storage.

407 Anticipated carbonate $\delta^{13}C$ values can be calculated using known temperature-dependent
408 equilibrium isotope fractionation factors between the different common carbonate minerals and
409 CO_2 (Table 4). The fractionation factor ($\alpha_{X\text{-}Y}$) describes the difference in isotopic composition
410 between two phases '*X*' and '*Y*':

411 (Eq. 1) $$\alpha_{X\text{-}Y} = R_X/R_Y = (\delta_X + 1000)/(\delta_Y + 1000)$$

412 where R_X and R_Y represent the $^{13}C/^{12}C$ ratios for phases *X* and *Y*, respectively, whereas δ_X and δ_Y
413 denote the per mil (‰) deviations of the $^{13}C/^{12}C$ ratios of phases *X* and *Y* in relation to a certified
414 reference material (VPDB):

415 (Eq. 2) $$\delta_X = 1000 \times \left[\frac{R_X - R_{VPDB}}{R_{VPDB}}\right] \text{ and } \delta_Y = 1000 \times \left[\frac{R_Y - R_{VPDB}}{R_{VPDB}}\right]$$

416 Carbon isotope ratio measurements are expressed as a per mil (‰) deviation from the
417 $^{13}C/^{12}C$ ratio of the VPDB international reference standard ($^{13}C/^{12}C_{VPDB}$ = 0.0112372; Allison et
418 al., 1995; Craig, 1957).

419 Fractionation factors ($\alpha_{X\text{-}Y}$) are related to temperature via equations of the form:

420 (Eq. 3) $$1000 \times \ln(\alpha_{X-Y}) = \frac{A \times 10^6}{T^2} + B \cong \delta_X - \delta_Y$$

421 where *T* is the temperature in degrees Kelvin, whereas *A* and *B* are regressed parameters.
422 Comprehensive reviews of these concepts can be found in Faure (1998) and Hoefs (2009).

Our calculations rely on the following constraints and assumptions: 1) The injected CO_2 plume becomes the dominant dissolved inorganic carbon (DIC) source in the storage system. The reservoir brine is initially acidified along zones of contact/interaction with the gradually expanding plume (however complex the interaction geometry may be; *e.g.,* Johnson et al., 2004; Kampman et al., 2014). At some distance away from the injection site, silicate mineral dissolution reactions eventually establish pH conditions that are conducive to carbonate precipitation and provide the necessary divalent cations (*e.g.,* Ca^{2+}, Mg^{2+}, Fe^{2+}) . Note that as the plume continues to expand over centuries to millennia, the carbonate cement volume that may have formed at some distance by the end of the first post-injection decade, for example, should re-dissolve and re-precipitate further away (*e.g.,* Liu et al., 2011). New cements are thus assumed to take on $\delta^{13}C$ values that reflect precipitation at an ambient reservoir temperature of ~50°C (Labotka et al., 2015) and the $\delta^{13}C$ the injected CO_2 (-9 to -11‰ at IBDP; Finley, 2005). Although the DIC pool in the IBDP reservoir has not been isotopically characterized, the low alkalinity of the Mt. Simon Formation brine (80 mg/L, as $CaCO_3$; Panno et al., 2013) suggests that upon interaction, the injected CO_2 will likely exert a primary control on the brine's isotopic composition. 2) The salinity/ionic composition of the reservoir brine (a Ca-Na-Cl type brine; Labotka et al., 2015) does not impart any secondary C-isotope fractionation effects during CO_2 dissolution. The current state of knowledge indicates that the influence of salinity on C-isotope partiotining between $CO_{2(g)}$ and DIC (*i.e.,* the 'salt-effect') is negligible (however this is not the case for O-isotopes); while studies in this field are still somewhat limited, Mayer et al. (2015) observe that "there is currently no evidence that these effects would significantly compromise the suitability of the stable isotopic composition of injected CO_2 as a tracer tool."

445 Using available data on carbon isotope partitioning between carbonates and $CO_{2(g)}$ (Table
446 4), we calculate the following approximate $\delta^{13}C$ values for newly-formed cements: -2‰ VPDB
447 for calcite (based on the work of Chacko et al., 1991), -6‰ for siderite (after Jimenez-Lopez and
448 Romanek, 2004), and -2‰ for dolomite-ankerite (based on the recent experimental work of
449 Horita (2014) for end-member dolomite; Fig. 3). A fractionation factor between $CO_{2(g)}$ and any
450 ankerite has not yet been experimentally calibrated, and it thus remains unknown how the Fe-
451 content in the dolomite-ankerite solid solution series affects equilibrium relations relative to end-
452 member dolomite. (Note that carbonate $\delta^{18}O$ values cannot be forecast at present because, to our
453 knowledge, the $\delta^{18}O$ of the supercritical CO_2 stream at the IBDP site has not been
454 determined/reported, although brine $\delta^{18}O$ values are known for various depths within the
455 reservoir unit; *e.g.,* Labotka et al., 2015).
456 How would these values be affected by primary carbonate cement dissolution and mixing
457 of the resulting $\delta^{13}C$ signal with that of the injected CO_2? At present we can only assess the
458 potential impact on newly formed dolomite, as calcite and siderite cements were not isotopically
459 characterized as part of this study (neither calcite nor siderite were encountered in the small
460 sample suite examined, although both are known constituents of the reservoir mineralogy; *e.g.,*
461 Palkovic, 2015). A bulk weighted average $\delta^{13}C$ value of -2.5‰ VPDB was calculated for the
462 representative patch of primary dolomite-ankerite cement shown in Fig. 3b. An image analysis
463 (using ImageJ software; Schneider et al., 2012) was performed to estimate the volume fraction
464 represented by each cement zone (Zones (1-3), 4, 5 and 6 respectively comprise 55%, 20%, 15%
465 and 10% of the total volume). Rapid and complete dissolution of this cement volume at 50°C
466 would, under the experimental conditions described by Horita (2014), produce $CO_{2\ (g)}$ with a

467 $\delta^{13}C$ value -11‰ VPDB. Thus, the impact of primary cement dissolution may not be discernable
468 considering that the $\delta^{13}C$ of the injected CO_2 stream varies between -9 to -11‰ VPDB.
469
470 **5. Part II: Broader Applications**
471 Here we attempt to identify some areas of current research interest where *in situ* isotope
472 microanalysis by SIMS could provide potentially unique insights to investigations concerned
473 with understanding how CO_2 will interact with geological reservoirs and caprocks under
474 engineered storage conditions. These include:
475 **1) Identifying sequestration-related carbonate cements in engineered CO_2-storage**
476 **reservoirs.** Only small cement volumes are anticipated in the initial years post-injection.
477 Nonetheless, as little as 3 micrometers (μm) of new growth could be readily analyzed by the
478 methodology described here, thus potentially providing early inputs for calibrating geochemical
479 models that attempt to predict how the mineralogy of a given reservoir-caprock system will
480 evolve in the long-term in response to imposed CO_2 storage (and to derive more accurate
481 estimates regarding the fraction of CO_2 that will become securely trapped in mineral form over
482 time). Hypothetically, it may also be necessary in future monitoring studies at CCS sites to
483 verify, via isotopic fingerprinting, whether fracture-filling cements in caprock units are related to
484 CO_2 leakage.
485
486 **2) Characterizing the carbonate components that pre-date CO_2-charging of natural and/or**
487 **engineered reservoirs.** Naturally-occurring accumulations of CO_2 in geological environments
488 are helping to build an understanding of how CO_2 interacts in the long-term (10^5-10^6 years) with
489 reservoir-caprock systems (*e.g.,* Bickle et al., 2013). Studies of these so-called natural analogues

aid, for example, in: 1) identifying the dominant fluid-mineral reactions that are expected to occur during engineered CO_2 storage; 2) allow for estimating rates of carbon mineralization; and 3) provide a means of calibrating geochemical models and reservoir simulations against the natural world (*e.g.,* Bickle et al., 2013; Higgs et al., 2015; Pearce et al., 1996; Sathaye et al., 2014; Stevens et al., 2001; Watson et al., 2004). As they relate to carbon sequestration in deep saline aquifers, the above three points have been identified as general knowledge gaps by the IPCC Special Report on CO_2 Capture and Storage (2005) (Michael et al., 2009). It was noted in a recent review of natural analogues that "a complete model of the fluid-mineral reactions will require both modeling of changes in fluid chemistry in conjunction with a full understanding of the petrology of the sandstone aquifer in which it will be essential to distinguish reaction products related to the present phase of [CO_2-charge related] alteration from earlier detrital and diagenetic phases" (Bickle et al., 2013). This point extends in relevance to the problem of determining the depth to which CO_2 penetrates into the caprock units that overlie natural reservoirs (as a means of assessing the likely long-term integrity of reservoir seals). Carbonate $\delta^{13}C$ and $\delta^{18}O$ signatures are a well-established tracer, although the ability of conventional methods to fully resolve isotopic differences among different end-member components can be hindered by small crystal size (*e.g.,* Lu et al., 2009) and/or if chemo-isotopic zonation is present at the micrometer scale (Heinemann et al., 2013; Wilkinson et al., 2009).

3) Characterizing experimental reaction products. This includes assessments of reservoir/caprock reactivity under simulated CO_2-storage conditions in cases where reaction product volumes are too small for conventional isotope ratio measurements. A further example is the problem of constraining equilibrium isotope fractionation factors between fluids and minerals

513 during precipitation. In experiments conducted at temperatures relevant to CO_2 storage in saline
514 aquifers (~50-150°C), precipitation rates are frustratingly slow for most common minerals.
515 Reaction product volumes that form over reasonable laboratory time-scales (months to several
516 years) are consequently quite small, as for example micrometer-scale overgrowths in instances
517 where seed crystals are used to stimulate mineral growth (*e.g.,* Pollington et al., 2016).
518
519 **4) Determining the carbon source(s) involved in carbonate cement-forming reactions in**
520 **sequestration environments other than deep saline aquifers.** Broadly speaking, many of the
521 carbon sequestration strategies currently under consideration (*e.g.,* Power et al., 2013) seek
522 efficient means (process routes) of converting CO_2 gas into carbonate minerals. Carbon
523 mineralization results in a product that is both environmentally benign and stable over geological
524 time scales. The fundamental idea underlying many strategies is essentially one of mimicking
525 natural geological processes (*e.g.,* silicate mineral weathering reactions or microbial
526 mineralization) and devising efficient engineering solutions aimed at accelerating the rate at
527 which these processes operate in controlled settings. Although such sequestration concepts are
528 still in the basic research and development stage, research efforts to date indicate that they could
529 be effective in substantially offsetting annual anthropogenic CO_2 emissions if deployed in
530 tandem on a sufficiently large scale. *In situ* carbonation of peridotite is one such strategy (*e.g.,*
531 Kelemen et al., 2011; Kelemen and Matter, 2008; Lackner et al., 1995; Matter and Kelemen,
532 2009). Promoting the carbonation of ultramafic mine tailings is another (*e.g.,* Wilson, 2006;
533 Wilson et al., 2009). It has been estimated, for example, that the annual sequestration capacity of
534 a large mine can exceed its annual CO_2 emissions (Power et al., 2013; Wilson, 2006).

Abundant in ultramafic mine tailings are Ca-Mg-Fe-rich silicate minerals (*e.g.,* olivine, pyroxene, plagioclase feldspars) that are thermodynamically unstable at Earth surface conditions; consequently, they weather rapidly. Carbonate minerals, particularly various forms of hydrated Mg-carbonates (*e.g.,* nesquehonite, dypingite, hydromagnesite, etc.), are among the common reaction products, forming crusts that may exhibit mineralogical and/or stable carbon isotope zonation (Wilson, 2006). In the case of micrometer-scale mineralogical banding, $\delta^{13}C$ zonation could reflect differences in the degree to which different hydrated Mg-carbonate species fractionate the stable isotopes of carbon during precipitation. It has also been recognized that different varieties of hydrated Mg-carbonates likely form via distinctly different pathways; some may be entirely abiotic in origin, whereas the precipitation of others may be microbially-mediated (Ferris et al., 1994; Power and Southam, 2005; Wilson et al., 2009). Understanding the relative efficiency of these end-member modes is significant for engineering efficient carbon mineralization systems, which may in the future rely in-part on microbial organisms that have been modified to locally accelerate the rate of silicate weathering and/or carbonate precipitation (Cappuccio et al., 2012; Chen et al., 2012; Ferris et al., 1994; Kamennaya et al., 2012; Krieger et al., 2012; Power et al., 2013). To this end, stable carbon and oxygen isotopic data, when used together with quantitative mineralogical analyses, can be an effective tool for identifying the carbon source(s) tapped during the formation of carbonate crusts (*e.g.,* atmospheric or biologically cycled CO_2, or carbon derived from dissolution of carbonate minerals in bedrock) and for quantifying the rate of their formation (*e.g.,* Wilson et al., 2009).

5. Concluding remarks

557 Stable carbon and oxygen isotope analyses ($\delta^{13}C$ and $\delta^{18}O$, respectively) are an important
558 component of research into CO_2-sequestration strategies, especially in so-called natural
559 analogues studies. Research efforts directed at natural analogues seek in-part to quantify the rate
560 and extent of CO_2-trapping via carbonate mineral cement formation (*i.e.,* carbon mineralization
561 or mineral-trapping of CO_2), and by so doing to make/refine quantitative predictions about the
562 probable long-term fate of CO_2 in prospective engineered reservoirs. Isotopic signatures (or
563 fingerprints) provide a means by which to distinguish different carbonate components present in
564 the reservoir-caprock system (*i.e.,* those that pre-date from those that post-date CO_2-charging).
565 However, clear interpretations of isotopic data acquired via conventional sampling
566 techniques in isotope ratio mass spectrometry (IRMS) (sampling typically at the 100-1000 μm^3
567 scale) can be significantly hindered in situations where it is not possible to mechanically or
568 chemically separate different carbonate components (due to small crystal size and/or the
569 presence of chemo-isotopic zoning at the micrometer scale).
570 Advances in secondary ion mass spectrometer (SIMS) instrument design, analytical
571 techniques and standardization have brought about the capability to routinely perform $\delta^{18}O$ and
572 $\delta^{13}C$ measurements *in situ* from sample domains as small as 1-10 μm across, with preservation of
573 the petrographic context of the analyzed sample volume. Many of the common Ca-Mg-Fe
574 carbonates can now be accurately analyzed, including the full spectrum of compositions along
575 the dolomite-ankerite and magnesite-siderite solid-solution series. These advances - many of
576 which have occurred since the time when geologic carbon sequestration was first proposed in
577 mid-1990's (Bachu et al., 1994; Lackner et al., 1995) and research into natural analogues began
578 (Pearce et al., 1996) – expand the potential analytical toolkit available to the research community
579 concerned with developing effective carbon sequestration strategies.

580 The analytical capability described here could provide potentially unique insights when
581 applied in studies concerned, for example, with following objectives (although this remains to be
582 critically evaluated):

583 • Verifying if, where, and at what rate carbonate cements precipitate in geological
584 reservoirs designated for engineered CO_2 storage;
585 • Characterizing the isotopic composition of carbonate components that pre-date the CO_2-
586 charge in engineered reservoirs or their natural analogues;
587 • Determining or refining existing rate estimates (based on bulk isotope analyses) of
588 carbonate cement-forming reactions in a variety of natural analogue environments;
589 • Analyzing the isotopic composition of experimental reaction products in instances where
590 product volumes are sufficiently small so as to hinder analysis by conventional IRMS
591 methods (this applies to laboratory-scale experiments designed to elucidate how CO_2
592 interacts with representative rock samples from a given reservoir-caprock system);

593

594 **Acknowledgments**

595 This material is based primarily upon work supported by the US Department of Energy Office of
596 Science, Office of Basic Energy Sciences, Chemical Sciences, Geosciences, and Biosciences
597 Division under award number DE-FG02-93ER14389. The WiscSIMS Laboratory is partly
598 funded by the US National Science Foundation (EAR-1355590). We thank our colleagues at the
599 University of Wisconsin-Madison for providing instrumentation support: N. Kita (SIMS), J.
600 Kern (SIMS), J. Fournelle (SEM & EPMA) and P. Gopon (SEM & EPMA). The Midwest
601 Geological Sequestration Consortium is acknowledged for making samples from the Illinois

602 Basin Decatur Project (IBDP) available for study and we thank A. Hyodo and the staff of the
603 Illinois State Geological Survey for assistance with sampling.

604

605 **References**

606 Alemu, B.L., Aagaard, P., Munz, I.A., Skurtveit, E., 2011. Caprock interaction with CO_2: A laboratory
607 study of reactivity of shale with supercritical CO_2 and brine. Appl. Geochem. 26, 1975–1989.
608 doi:10.1016/j.apgeochem.2011.06.028
609 Allison, C.E., Francey, R.J., Meijer, H.A.J., 1995. Recommendations for the reporting of stable isotope
610 measurements of carbon and oxygen in CO_2 gas, in: Reference and Intercomparison Materials for
611 Stable Isotopes of Light Elements. Presented at the Reference and Intercomparison Materials for
612 Stable Isotopes of Light Elements, International Atomic Energy Agency, Vienna, Austria, pp.
613 155–162.
614 Bachu, S., Gunter, W.D., Perkins, E.H., 1994. Aquifer disposal of CO_2: Hydrodynamic and mineral
615 trapping. Energy Convers. Manag. 35, 269–279. doi:10.1016/0196-8904(94)90060-4
616 Baines, S.J., Worden, R.H., 2004a. Geological storage of carbon dioxide. Geol. Soc. Lond. Spec. Publ.
617 233, 1–6.
618 Baines, S.J., Worden, R.H., 2004b. The long-term fate of CO_2 in the subsurface: natural analogues for
619 CO_2 storage. Geol. Soc. Lond. Spec. Publ. 233, 59–85.
620 Bickle, M., Kampman, N., Wigley, M., 2013. Natural Analogues. Rev. Mineral. Geochem. 77, 15–71.
621 doi:10.2138/rmg.2013.77.2
622 Bickle, M.J., 2009. Geological carbon storage. Nat. Geosci. 2, 815–818. doi:10.1038/ngeo687
623 Bonneville, A., Gilmore, T., Sullivan, C., Vermeul, V., Kelley, M., White, S., Appriou, D., Bjornstad, B.,
624 Gerst, J., Gupta, N., Horner, J., McNeil, C., Moody, M., Rike, W., Spane, F., Thorne, P., Zeller,
625 E., Zhang, F., Hoffmann, J., Humphreys, K., 2013. Evaluating the Suitability for CO_2 Storage at
626 the FutureGen 2.0 Site, Morgan County, Illinois, USA. Energy Procedia 37, 6125–6132.
627 doi:10.1016/j.egypro.2013.06.541
628 Bowen, B.B., Ochoa, R.I., Wilkens, N.D., Brophy, J., Lovell, T.R., Fischietto, N., Medina, C.R., Rupp,
629 J.A., 2011. Depositional and diagenetic variability within the Cambrian Mount Simon Sandstone:
630 Implications for carbon dioxide sequestration. Environ. Geosci. 18, 69–89.
631 doi:10.1306/eg.07271010012
632 Burley, S.D., Kantorowicz, J.D., 1986a. Thin section and SEM textural criteria for the recognition of
633 cement-dissolution porosity in sandstones. Sedimentology 33, 587–604.

634 Burley, S.D., Kantorowicz, J.D., 1986b. Reply. Sedimentology 33, 608–614. doi:10.1111/j.1365-
635 3091.1986.tb00765.x
636 Cappuccio, J.A., Lui, G.V., Pillar, V.D., Ajo-Franklin, C.M., 2012. Tuning Microbial Surfaces to Control
637 Carbonate Mineralization. Biophys. J. 102, 188a. doi:10.1016/j.bpj.2011.11.1024
638 Carroll, S.A., McNab, W.W., Dai, Z., Torres, S.C., 2013. Reactivity of Mount Simon Sandstone and the
639 Eau Claire Shale Under CO_2 Storage Conditions. Environ. Sci. Technol. 47, 252–261.
640 doi:10.1021/es301269k
641 Celia, M.A., Bachu, S., Nordbotten, J.M., Bandilla, K.W., 2015. Status of CO_2 storage in deep saline
642 aquifers with emphasis on modeling approaches and practical simulations. Water Resour. Res. 51,
643 6846–6892. doi:10.1002/2015WR017609
644 Chacko, T., Mayeda, T.K., Clayton, R.N., Goldsmith, J.R., 1991. Oxygen and carbon isotope
645 fractionations between CO_2 and calcite. Geochim. Cosmochim. Acta 55, 2867–2882.
646 doi:10.1016/0016-7037(91)90452-B
647 Chang, L.L., Howie, R.A., Zussman, J., 1998. , in: Non-Silicates: Sulphates, Carbonates, Phosphates,
648 Halides. Harlow, Longman Group Limited, p. 383.
649 Chen, P.-H., Liu, H.-L., Chen, Y.-J., Cheng, Y.-H., Lin, W.-L., Yeh, C.-H., Chang, C.-H., 2012.
650 Enhancing CO_2 bio-mitigation by genetic engineering of cyanobacteria. Energy Environ. Sci. 5,
651 8318–8327. doi:10.1039/c2ee21124f
652 Craig, H., 1957. Isotopic standards for carbon and oxygen and correction factors for mass-spectrometric
653 analysis of carbon dioxide. Geochim. Cosmochim. Acta 12, 133–149.
654 DePaolo, D.J., Cole, D.R., 2013. Geochemistry of Geologic Carbon Sequestration: An Overview. Rev.
655 Mineral. Geochem. 77, 1–14. doi:10.2138/rmg.2013.77.1
656 DOE, 2010. Carbon sequestration ATLAS of the United States and Canada. Off. Foss. Energy Natl.
657 Energy Technol. Lab. Morgant. WV 90p.
658 Eiler, J.M., Valley, J.W., Graham, C.M., 1997. Standardization of SIMS analysis of O and C isotope
659 ratios in carbonates from ALH84001, in: Lunar and Planetary Science Conference. p. 327.
660 Faure, G., 1998. Principles and applications of geochemistry: a comprehensive textbook for geology
661 students. Prentice Hall.
662 Ferris, F., Wiese, R., Fyfe, W., 1994. Precipitation of Carbonate Minerals by Microorganisms -
663 Implications for Silicate Weathering and the Global Carbon-Dioxide Budget. Geomicrobiol. J.
664 12, 1–13.
665 Finley, R., 2005. An assessment of geological carbon sequestration options in the Illinois Basin. United
666 States. Department of Energy.

667 Fishman, N.S., 1997. Basin-wide fluid movement in a Cambrian paleoaquifer: evidence from the Mt.
668 Simon sandstone, Illinois and Indiana, in: Montanez, I.P., Gregg, J.M., Shelton, K.L. (Eds.),
669 Basin-Wide Diagenetic Patterns: Integrated Petrologic, Geochemical, and Hydrologic
670 Considerations. SEPM (Society for Sedimentary Geology), Tulsa, Oklahoma, U.S.A., pp. 221–
671 234.
672 Gale, J., 2004. Why do we need to consider geological storage of CO_2. Geol. Soc. Lond. Spec. Publ. 233,
673 7–15. doi:10.1144/GSL.SP.2004.233.01.02
674 Gibbins, J., Chalmers, H., 2008. Carbon capture and storage. Energy Policy 36, 4317–4322.
675 doi:10.1016/j.enpol.2008.09.058
676 Gunter, W.D., Bachu, S., Benson, S., 2004. The role of hydrogeological and geochemical trapping in
677 sedimentary basins for secure geological storage of carbon dioxide. Geol. Soc. Lond. Spec. Publ.
678 233, 129–145.
679 Haszeldine, R.S., Quinn, O., England, G., Wilkinson, M., Shipton, Z.K., Evans, J.P., Heath, J., Crossey,
680 L., Ballentine, C.J., Graham, C.M., 2005. Natural geochemical analogues for carbon dioxide
681 storage in deep geological porous reservoirs, a United Kingdom perspective. Oil Gas Sci.
682 Technol. 60, 33–49.
683 Heinemann, N., Wilkinson, M., Haszeldine, R.S., Fallick, A.E., Pickup, G.E., 2013. CO_2 sequestration in
684 a UK North Sea analogue for geological carbon storage. Geology 41, 411–414.
685 doi:10.1130/G33835.1
686 Hervig, R.L., Williams, P., Thomas, R.M., Schauer, S.N., Steele, I.M., 1992. Microanalysis of oxygen
687 isotopes in insulators by secondary ion mass spectrometry. Int. J. Mass Spectrom. Ion Process.
688 120, 45–63.
689 Higgs, K.E., Haese, R.R., Golding, S.D., Schacht, U., Watson, M.N., 2015. The Pretty Hill Formation as
690 a natural analogue for CO_2 storage: An investigation of mineralogical and isotopic changes
691 associated with sandstones exposed to low, intermediate and high CO_2 concentrations over
692 geological time. Chem. Geol., Measuring and predicting the geochemical impacts of CO_2 storage
693 on reservoir rocks 399, 36–64. doi:10.1016/j.chemgeo.2014.10.019
694 Hoefs, J., 2009. Stable isotope geochemistry, 6th ed. Springer-Verlag Berlin Heidelberg.
695 Hoffert, M.I., Caldeira, K., Benford, G., Criswell, D.R., Green, C., Herzog, H., Jain, A.K., Kheshgi, H.S.,
696 Lackner, K.S., Lewis, J.S., others, 2002. Advanced technology paths to global climate stability:
697 energy for a greenhouse planet. science 298, 981–987.
698 Hoholick, J.D., Metarko, T., Potter, P.E., 1984. Regional variations of porosity and cement: St. Peter and
699 Mount Simon sandstones in Illinois Basin. AAPG Bull. 68, 753–764.

700 Horita, J., 2014. Oxygen and carbon isotope fractionation in the system dolomite–water–CO_2 to elevated
701 temperatures. Geochim. Cosmochim. Acta 129, 111–124. doi:10.1016/j.gca.2013.12.027
702 Hosa, A., Esentia, M., Stewart, J., Haszeldine, S., 2011. Injection of CO_2 into saline formations:
703 Benchmarking worldwide projects. Chem. Eng. Res. Des. 89, 1855–1864.
704 doi:10.1016/j.cherd.2011.04.003
705 Hyodo, A., Kozdon, R., Pollington, A.D., Valley, J.W., 2014. Evolution of quartz cementation and burial
706 history of the Eau Claire Formation based on in situ oxygen isotope analysis of quartz
707 overgrowths. Chem. Geol. 384, 168–180. doi:10.1016/j.chemgeo.2014.06.021
708 IPCC Special Report on Carbon Dioxide Capture and Storage, 2005. Cambridge University Press, for the
709 Intergovernmental Panel on Climate Change, Cambridge.
710 Jimenez-Lopez, C., Romanek, C.S., 2004. Precipitation kinetics and carbon isotope partitioning of
711 inorganic siderite at 25°C and 1 atm. Geochim. Cosmochim. Acta 68, 557–571.
712 doi:10.1016/S0016-7037(03)00460-5
713 Johnson, J.W., Nitao, J.J., Knauss, K.G., 2004. Reactive transport modelling of CO_2 storage in saline
714 aquifers to elucidate fundamental processes, trapping mechanisms and sequestration partitioning.
715 Geological Society, London, Special Publications 233, 107–128.
716 Kaldi, J., Daniel, R., Tenthorey, E., Michael, L., Schacht, U., Nicol, A., Undershultz, J., Backé, G., 2011.
717 Caprock systems for CO_2 geological storage. Cooperative Research Centre for Greenhouse Gas
718 Technlogies, Canberra, ACT, CO2CRC Publication Number RPT10-2774.
719 Kamennaya, N., Ajo-Franklin, C., Northen, T., Jansson, C., 2012. Cyanobacteria as Biocatalysts for
720 Carbonate Mineralization. Minerals 2, 338–364. doi:10.3390/min2040338
721 Kampman, N., Bickle, M., Wigley, M., Dubacq, B., 2014. Fluid flow and CO_2–fluid–mineral interactions
722 during CO_2-storage in sedimentary basins. Chemical Geology 369, 22–50.
723 doi:10.1016/j.chemgeo.2013.11.012
724
725 Kelemen, P.B., Matter, J., 2008. In situ carbonation of peridotite for CO_2 storage. Proc. Natl. Acad. Sci.
726 105, 17295–17300.
727 Kelemen, P.B., Matter, J., Streit, E.E., Rudge, J.F., Curry, W.B., Blusztajn, J., 2011. Rates and
728 Mechanisms of Mineral Carbonation in Peridotite: Natural Processes and Recipes for Enhanced,
729 in situ CO_2 Capture and Storage. Annu. Rev. Earth Planet. Sci. 39, 545–576.
730 doi:10.1146/annurev-earth-092010-152509
731 Kelly, J.L., Fu, B., Kita, N.T., Valley, J.W., 2007. Optically continuous silcrete quartz cements of the St.
732 Peter Sandstone: High precision oxygen isotope analysis by ion microprobe. Geochim.
733 Cosmochim. Acta 71, 3812–3832. doi:10.1016/j.gca.2007.05.014

734 Kita, N.T., Ushikubo, T., Fu, B., Valley, J.W., 2009. High precision SIMS oxygen isotope analysis and
735 the effect of sample topography. Chem. Geol. 264, 43–57.
736 Kolata, D.R., Nimz, C.K., 2010. Geology of Illinois. University of Illinois at Urbana-Champaign,
737 Institute of Natural Resource Sustainability, Illinois State Geological Survey, Champaign,
738 Illinois.
739 Krieger, K., 2012. Genetically Engineered Bacteria Could Help Fight Climate Change [WWW
740 Document]. URL http://www.sciencemag.org/news/2012/02/genetically-engineered-bacteria-
741 could-help-fight-climate-change (accessed 3.8.16).
742 Labotka, D.M., Panno, S.V., Locke, R.A., Freiburg, J.T., 2015. Isotopic and geochemical characterization
743 of fossil brines of the Cambrian Mt. Simon Sandstone and Ironton–Galesville Formation from the
744 Illinois Basin, USA. Geochim. Cosmochim. Acta 165, 342–360. doi:10.1016/j.gca.2015.06.013
745 Lackner, K.S., 2003. A guide to CO_2 sequestration. Science 300, 1677–1678.
746 Lackner, K.S., Wendt, C.H., Butt, D.P., Joyce Jr., E.L., Sharp, D.H., 1995. Carbon dioxide disposal in
747 carbonate minerals. Energy 20, 1153–1170. doi:10.1016/0360-5442(95)00071-N
748 Leetaru, H.E., Frailey, S., Morse, D., Finley, R.J., Rupp, J.A., Drahozval, J.A., McBride, J.H., 2009.
749 Carbon sequestration in the Mt. Simon Sandstone saline reservoir.
750 Leetaru, H.E., Freiburg, J.T., 2014. Litho-facies and reservoir characterization of the Mt Simon Sandstone
751 at the Illinois Basin - Decatur Project: Litho-facies and reservoir characterization of the Mt Simon
752 Sandstone at the Illinois Basin. Greenh. Gases Sci. Technol. 4, 580–595. doi:10.1002/ghg.1453
753 Liu, F., Lu, P., Griffith, C., Hedges, S.W., Soong, Y., Hellevang, H., Zhu, C., 2012. CO_2–brine–caprock
754 interaction: Reactivity experiments on Eau Claire shale and a review of relevant literature. Int. J.
755 Greenh. Gas Control 7, 153–167. doi:10.1016/j.ijggc.2012.01.012
756 Liu, F., Lu, P., Zhu, C., Xiao, Y., 2011. Coupled reactive flow and transport modeling of CO_2
757 sequestration in the Mt. Simon sandstone formation, Midwest U.S.A. Int. J. Greenh. Gas Control
758 5, 294–307. doi:10.1016/j.ijggc.2010.08.008
759 Lu, J., Wilkinson, M., Haszeldine, R.S., Boyce, A.J., 2011. Carbonate cements in Miller field of the UK
760 North Sea: a natural analog for mineral trapping in CO_2 geological storage. Environ. Earth Sci.
761 62, 507–517. doi:10.1007/s12665-010-0543-1
762 Lu, J., Wilkinson, M., Haszeldine, R.S., Fallick, A.E., 2009. Long-term performance of a mudrock seal in
763 natural CO_2 storage. Geology 37, 35–38. doi:10.1130/G25412A.1
764 Machel, H.G., 1997. Recrystallization versus neomorphism, and the concept of "significant
765 recrystallization"in dolomite research. Sediment. Geol. 113, 161–168.
766 Matter, J.M., Kelemen, P.B., 2009. Permanent storage of carbon dioxide in geological reservoirs by
767 mineral carbonation. Nat. Geosci. 2, 837–841. doi:10.1038/ngeo683

768 Matter, J.M., Stute, M., Snæbjörnsdottir, S.Ó., Oelkers, E.H., Gislason, S.R., Aradottir, E.S., Sigfusson,
769 B., Gunnarsson, I., Sigurdardottir, H., Gunnlaugsson, E., Axelsson, G., Alfredsson, H.A., Wolff-
770 Boenisch, D., Mesfin, K., Taya, D.F. de la R., Hall, J., Dideriksen, K., Broecker, W.S., 2016.
771 Rapid carbon mineralization for permanent disposal of anthropogenic carbon dioxide emissions.
772 Science 352, 1312–1314. doi:10.1126/science.aad8132
773 Mayer, B., Humez, P., Becker, V., Dalkhaa, C., Rock, L., Myrttinen, A., Barth, J.A.C., 2015. Assessing
774 the usefulness of the isotopic composition of CO_2 for leakage monitoring at CO_2 storage sites: A
775 review. Int. J. Greenh. Gas Control 37, 46–60. doi:10.1016/j.ijggc.2015.02.021
776 McGrail, B.P., Schaef, H.T., Ho, A.M., Chien, Y.-J., Dooley, J.J., Davidson, C.L., 2006. Potential for
777 carbon dioxide sequestration in flood basalts. J. Geophys. Res. Solid Earth 111, 1–13.
778 Michael, K., Arnot, M., Cook, P., Ennis-King, J., Funnell, R., Kaldi, J., Kirste, D., Paterson, L., 2009.
779 CO_2 storage in saline aquifers I—Current state of scientific knowledge. Energy Procedia 1, 3197–
780 3204. doi:10.1016/j.egypro.2009.02.103
781 Michael, K., Golab, A., Shulakova, V., Ennis-King, J., Allinson, G., Sharma, S., Aiken, T., 2010.
782 Geological storage of CO_2 in saline aquifers-A review of the experience from existing storage
783 operations. Int. J. Greenh. Gas Control 4, 659–667. doi:10.1016/j.ijggc.2009.12.011
784 Morad, S., 2009. Carbonate Cementation in Sandstones: Distribution Patterns and Geochemical Evolution
785 (Special Publication 26 of the IAS). John Wiley & Sons.
786 Neufelder, R.J., Bowen, B.B., Lahann, R.W., Rupp, J.A., 2012. Lithologic, mineralogical, and
787 petrophysical characteristics of the Eau Claire Formation: Complexities of a carbon storage
788 system seal. Environ. Geosci. 19, 81–104. doi:10.1306/eg.02081211014
789 Orr, F.M., 2009. CO_2 capture and storage: are we ready? Energy Environ. Sci. 2, 449–458.
790 doi:10.1039/b822107n
791 Page, F.Z., Ushikubo, T., Kita, N.T., Riciputi, L.R., Valley, J.W., 2007. High-precision oxygen isotope
792 analysis of picogram samples reveals 2 μm gradients and slow diffusion in zircon. Am. Mineral.
793 92, 1772–1775. doi:10.2138/am.2007.2697
794 Palkovic, M.J., 2015. Depositional characterization of the Eau Claire Formation at the Illinois Basin–
795 Decatur Project: facies, mineralogy and geochemistry (Ms.c). University of Illinois at Urbana-
796 Champaign.
797 Panno, S.V., Hackley, K.C., Locke, R.A., Krapac, I.G., Wimmer, B., Iranmanesh, A., Kelly, W.R., 2013.
798 Formation waters from Cambrian-age strata, Illinois Basin, USA: Constraints on their origin and
799 evolution. Geochim. Cosmochim. Acta 122, 184–197. doi:10.1016/j.gca.2013.08.021
800 Pearce, J.M., Holloway, S., Wacker, H., Nelis, M.K., Rochelle, C., Bateman, K., 1996. Natural
801 occurrences as analogues for the geological disposal of carbon dioxide. Energy Convers. Manag.,

802 Proceedings of the International Energy Agency Greenhouse Gases: Mitigation Options
803 Conference 37, 1123–1128. doi:10.1016/0196-8904(95)00309-6
804 Pollington, A.D., Kozdon, R., Anovitz, L.M., Georg, R.B., Spicuzza, M.J., Valley, J.W., 2016.
805 Experimental calibration of silicon and oxygen isotope fractionations between quartz and water at
806 250°C by in situ microanalysis of experimental products and application to zoned low δ30Si
807 quartz overgrowths. Chem. Geol. 421, 127–142. doi:10.1016/j.chemgeo.2015.11.011
808 Pollington, A.D., Kozdon, R., Valley, J.W., 2011. Evolution of quartz cementation during burial of the
809 Cambrian Mount Simon Sandstone, Illinois Basin: In situ microanalysis of $\delta^{18}O$. Geology 39,
810 1119–1122.
811 Power, I., Southam, G., 2005. Carbon dioxide sequestration through enhanced weathering of chrysotile
812 mine tailings and subsequent microbial precipitation of magnesium carbonates. Geochim.
813 Cosmochim. Acta Suppl. 69, 834.
814 Power, I.M., Harrison, A.L., Dipple, G.M., Wilson, S.A., Kelemen, P.B., Hitch, M., Southam, G., 2013.
815 Carbon Mineralization: From Natural Analogues to Engineered Systems. Rev. Mineral.
816 Geochem. 77, 305–360. doi:10.2138/rmg.2013.77.9
817 Rowan, E.L., Goldhaber, M.B., Hatch, J.R., 2002. Regional fluid flow as a factor in the thermal history of
818 the Illinois basin: Constraints from fluid inclusions and the maturity of Pennsylvanian coals.
819 AAPG Bull. 86, 257–277.
820 Sathaye, K.J., Hesse, M.A., Cassidy, M., Stockli, D.F., 2014. Constraints on the magnitude and rate of
821 CO_2 dissolution at Bravo Dome natural gas field. Proc. Natl. Acad. Sci. 111, 15332–15337.
822 Schneider, C.A., Rasband, W.S., Eliceiri, K.W., 2012. "NIH Image to ImageJ: 25 years of image
823 analysis", Nat methods 9, 671-675.
824 Śliwiński, M.G., Kitajima, K., Kozdon, R., Spicuzza, M.J., Fournelle, J.H., Denny, A., Valley, J.W.,
825 2015a. Secondary Ion Mass Spectrometry Bias on Isotope Ratios in Dolomite–Ankerite, Part I:
826 $\delta^{18}O$ Matrix Effects. Geostand. Geoanalytical Res. n/a-n/a. doi:10.1111/j.1751-
827 908X.2015.00364.x
828 Śliwiński, M.G., Kitajima, K., Kozdon, R., Spicuzza, M.J., Fournelle, J.H., Denny, A., Valley, J.W.,
829 2015b. Secondary Ion Mass Spectrometry Bias on Isotope Ratios in Dolomite–Ankerite, Part II:
830 $\delta^{13}C$ Matrix Effects. Geostand. Geoanalytical Res. doi:10.1111/j.1751-908X.2015.00380.x
831 Sliwinski, M.G., Kozdon, R., Kitajima, K., Denny, A., Spicuzza, M., Valley, J.W., 2015c. In-Situ,
832 Micron-Scale $\delta^{13}C$ & $\delta^{18}O$ Analyses (by SIMS) of Chemo-Isotopically Zoned Carbonate Cements
833 of Diagenetic Origin — A Case Study on the Implications for the Thermal and Burial History of
834 the Eau Claire Fm., Illinois Basin (USA). AAPG Annual Convention and Exhibition, Denver,
835 Colorado, 31 May – 1 June. AAPG Search and Discovery URL:

836 Śliwiński, M.G., Kozdon, R., Kitajima, K., Denny, A., Valley, J.W., 2016. Microanalysis of carbonate
837 cement $\delta^{18}O$ in a CO_2-storage system seal: Insights into the diagenetic history of the Eau Claire
838 Formation (Upper Cambrian), Illinois Basin. AAPG Bull. 100, 1003–1031.
839 Stevens, S.H., Pearce, J.M., Rigg, A.A.J., 2001. Natural analogs for geologic storage of CO_2: An
840 integrated global research program, in: Proceedings of the First National Conference of Carbon
841 Sequestration, National Energy Technology Laboratory, Washington, DC, USA.
842 Valley, J.W., Kita, N.T., 2009. In situ oxygen isotope geochemistry by ion microprobe, in: Fayek, M.
843 (Ed.), Secondary Ion Mass Spectrometry in the Earth Sciences: Gleaning the Big Picture from a
844 Small Spot. Mineralogical Association of Canada (MAC), pp. 19–63.
845 Vermeul, V.R., Amonette, J.E., Strickland, C.E., Williams, M.D., Bonneville, A., 2016. An overview of
846 the monitoring program design for the FutureGen 2.0 CO_2 storage site. International Journal of
847 Greenhouse Gas Control 51, 193–206. doi:10.1016/j.ijggc.2016.05.023
848 Watson, M.N., Zwingmann, N., Lemon, N.M., 2004. The Ladbroke Grove–Katnook carbon dioxide
849 natural laboratory: A recent CO_2 accumulation in a lithic sandstone reservoir. Energy, 6th
850 International Conference on Greenhouse Gas Control Technologies 29, 1457–1466.
851 doi:10.1016/j.energy.2004.03.079
852 Wigley, T.M., Richels, R., Edmonds, J.A., 1996. Economic and environmental choices in the stabilization
853 of atmospheric CO_2 concentrations. Nature 379, 240–243.
854 Wilkinson, M., Haszeldine, R.S., Fallick, A.E., Odling, N., Stoker, S.J., Gatliff, R.W., 2009. CO_2-Mineral
855 Reaction in a Natural Analogue for CO_2 Storage--Implications for Modeling. J. Sediment. Res.
856 79, 486–494. doi:10.2110/jsr.2009.052
857 Wilson, S.A., Raudsepp, M., Dipple, G.M., 2006. Verifying and quantifying carbon fixation in minerals
858 from serpentine-rich mine tailings using the Rietveld method with X-ray powder diffraction data.
859 Am. Mineral. 91, 1331–1341. doi:10.2138/am.2006.2058
860 Wilson, S.A., Dipple, G.M., Power, I.M., Thom, J.M., Anderson, R.G., Raudsepp, M., Gabites, J.E.,
861 Southam, G., 2009. Carbon dioxide fixation within mine wastes of ultramafic-hosted ore deposits:
862 Examples from the Clinton Creek and Cassiar chrysotile deposits, Canada. Econ. Geol. 104, 95–
863 112.
864 Yoksoulian, L.E., Freiburg, J.T., Butler, S.K., Berger, P.M., Roy, W.R., 2013. Mineralogical Alterations
865 During Laboratory-scale Carbon Sequestration Experiments for the Illinois Basin. Energy
866 Procedia 37, 5601–5611. doi:10.1016/j.egypro.2013.06.482
867
868

FIGURE AND TABLE CAPTIONS

Fig. 1. (A) Locations of drill holes sampled for this study of the upper Mt. Simon Sandstone and the overlying Eau Claire shale. These units respectively comprise the reservoir and the caprock (impermeable seal) at the Illinois Basin Decatur Project (IBDP), a demonstration site for the feasibility of engineered, long-term injection and storage of anthropogenic CO_2 in a deep saline aquifer. Geographic extent of Illinois Basin traced after Kolata and Nimz (2010). (B) Cambrian stratigraphy of the Illinois Basin (north of latitude 40°N); only the portion that is relevant to this study is shown. Modified after Kolata (2005).

Fig. 2. From core to in situ isotope microanalysis of mineral cements. Segments of core showing (A) the shaly Eau Claire Formation, the primary reservoir at IBDP (well C13637, depth interval: 1095-1097 m / 3592-3598.5 feet) and (B) the upper Mt. Simon sandstone reservoir at the Illinois Basin Decatur Project site (ADM Verification Well #1, depth interval: 1678-1679.5 m / 5505-5510 feet; see Fig. 1). (Image in (B) modified after Fig. 4.1 in Palkovic, 2015). Sample preparation at WiscSIMS involves casting a small subsample of core (~1 cm^3 from C) into a 1-inch (25-mm) diameter epoxy mount (D) and co-mounting an appropriate reference material (RM) in the center. Areas of interest for analysis (*e.g.,* 'A11' in D; see also SA 1) are identified by BSE-SEM-imaging (the quartz-grain framework of this sample is uniformly dark gray in this image, whereas the light-gray shades represent pore-filling, chemically zoned dolomite-ankerite cements. Pyrite and K-feldspar appear white.)

Fig. 3. Preliminary pre-injection characterization by *in situ* isotope microanalysis of the stable carbon and oxygen isotope compositions ($\delta^{13}C$ and $\delta^{18}O$, respectively) of individual dolomite-ankerite cement zones in the IBDP reservoir-caprock system (analysis performed by secondary ion mass spectrometry – SIMS; note the analysis pits in A and B). BSE-SEM images showing dolomite-ankerite cements (Dol-Ank) exhibiting micrometer-scale chemo-isotopic zoning in samples of: (A) the Eau Claire shale (Core 13637, depth = 1096.5 m / 3597.5 ft; see Fig. 1) and (B) the upper Mt. Simon Sandstone (ADM Verification Well #1, depth = 1680.4 m / 5513.2 ft; see Fig. 1), along with corresponding isotopic data (C). Fe-bearing domains appear brighter in these images. Note that due to sampling restrictions, the Eau Claire was sampled from core in a nearby county (~75 km WSW of the IBDP site). Arrows labeled "Dol-Ank" and "Sd" (siderite) in (C) indicate the anticipated $\delta^{13}C$ values of new carbonates that are expected to form in response to long-term CO_2 storage (see Section 4.1 and Table 4). DF+OF = detrital K-feldspar with diagenetic overgrowths; Qtz = Quartz.

Fig. 4. Select geochemical characteristics of individual carbonate and quartz cement zones within the upper Mt. Simon Sandstone (IBDP, ADM Verification Well #1, depth = 1680.4 m / 5513.2 ft). (A) Ca-Mg-Fe ternary diagram showing the cation composition of each major dolomite-ankerite cement zone along with the corresponding (B) Fe/Mg ratios (expressed as the Fe#, or molar Fe/[Mg+Fe]) and stable isotope composition of oxygen ($\delta^{18}O$; C) and carbon ($\delta^{13}C$; D). (E) $\delta^{18}O$ values of individual quartz-overgrowth cement zones. (F) Relative sequence of quartz and carbonate cement zone development. For each cement zone depicted in (B-E), datapoints are offset relative to one another only for clarity.

Fig. 5. (A) BSE-SEM image showing chemo-isotopically zoned dolomite-ankerite cements (Dol-Ank) in a sample of the Eau Claire shale and representative SIMS isotope microanalysis pits (6-µm $\delta^{13}C$ and 10-µm $\delta^{18}O$). Fe-bearing domains appear brighter. (Core 13637, depth = 1096.5 m / 3597.5 ft). Z0, Z1a, Z1b, Z2a, Z2b, Z3 = carbonate cement zones. DF+OF = detrital K-feldspar with diagenetic overgrowths; Qtz = Quartz

Fig. 6. Select geochemical characteristics of individual carbonate cement zones within the Eau Claire shale (Core 13637, depth = 1096.5 m / 3597.5 ft). (A) Ca-Mg-Fe ternary diagram showing the cation composition of each major dolomite-ankerite cement zone along with the corresponding (B) Fe/Mg ratios (expressed as the Fe#, or molar Fe/(Mg+Fe)) and stable isotope composition of oxygen ($\delta^{18}O$, C) and carbon ($\delta^{13}C$, D). For each cement zone depicted in (B-D), datapoints are offset relative to one another only for clarity.

Fig. 7. Corresponding BSE-SEM and CL-SEM images showing the microstratigraphic relationships among the different generations of quartz and carbonate cements identified within the upper Mt. Simon Sandstone (IBDP, ADM Verification Well#1, depth = 1680.4 m / 5513.2 ft). Six major stages of carbonate cementation (Dol-Ank = dolomite-ankerite) and four distinct quartz-overgrowth (QO) generations were observed within the examined sample. DQ = detrital quartz; OF = overgrowth feldspar.

935 **Table 1.** Isotopic composition ($\delta^{13}C$ and $\delta^{18}O$ by SIMS) and major element chemistry (by
936 EPMA) of carbonate cements in the upper Mt. Simon Sandstone (ADM Verification Well #1,
937 depth = 1680.4 m / 5513.2 ft). Refer to SA 1 for petrographic context of each spot-analysis.
938
939 **Table 2.** Isotopic composition ($\delta^{13}C$ and $\delta^{18}O$ by SIMS) and major element chemistry (by
940 EPMA) of carbonate cements in the Eau Claire shale (C13637, depth = 1096.5 m / 3597.5 ft).
941 Refer to SA 1 for petrographic context of each spot-analysis.
942
943 **Table 3.** Isotopic composition ($\delta^{18}O$ by SIMS) of quartz-overgrowths in the upper Mt. Simon
944 Sandstone (ADM Verification Well #1; depth = 1680.4 m / 5513.2 ft). Refer to SA 1 for
945 petrographic context of each spot-analysis.
946
947 **Table 4.** Predicted C-isotope composition of sequestration-related carbonate cements at the
948 Illinois Basin Decatur Project site.
949
950 **Supplemental Appendix 1.** Petrographic documentation of all sample regions analyzed by
951 SIMS (*in situ*, micron-scale $\delta^{18}O$ and $\delta^{13}C$ analyses), with individually annotated analysis pits.
952
953 **Supplemental Appendix 2.** Complete SIMS data table: 10-µm spot-size O-isotope
954 measurements.
955
956 **Supplemental Appendix 3.** Complete SIMS data table: 3-µm spot-size O-isotope
957 measurements.

Supplemental Appendix 4. Complete SIMS data table: 6-µm spot-size C-isotope measurements.

Table 1: Isotopic composition ($\delta^{13}C$ and $\delta^{18}O$)of carbonate cements in the upper Mount Simon Sandstone (ADM Verification Well #1, depth = 5513.2 ft)

Session specific sample I.D.	SIMS session	Sample region i.d.	Spot-size (μm)	$\delta^{18}O$‰ PDB	$\delta^{18}O$‰ V-SMOW	2SD	Session specific sample I.D.	$\delta^{13}C$‰ PDB	2SD	Zone	Fe#	$MgCO_3$ (mol.%)	$CaCO_3$ (mol.%)	$FeCO_3$ (mol.%)	$MnCO_3$ (mol.%)
20140513@598.asc	S7	Area 11	10	-8.4	22.3	0.4	20140404@268.asc	-3.2	1.1	1	0.231	39.04	48.14	11.75	1.08
20140513@595.asc	S7	Area 11	10	-12.3	18.2	0.4	20140404@269.asc	-2.8	1.1	1	0.238	35.37	50.59	11.07	2.97
20140513@599.asc	S7	Area 11	10	-9.9	20.7	0.4	20140404@269.asc	-2.8	1.1	1	0.238	35.37	50.59	11.07	2.97
20140513@597.asc	S7	Area 11	10	-8.9	21.8	0.4	20140404@267.asc	-1.5	1.1	1	0.228	38.53	49.42	11.40	0.66
20140513@596.asc	S7	Area 11	10	-9.1	21.5	0.4	20140404@270.asc	-1.5	1.1	1	0.208	39.20	49.95	10.27	0.59
20140513@607.asc	S7	Area 11	10	-10.2	20.3	0.3	20140404@271.asc	-0.4	1.1	2	0.197	39.57	50.18	9.70	0.55
20140513@606.asc	S7	Area 11	10	-10.3	20.3	0.3	20140404@272.asc	-0.5	1.1	2	0.200	40.90	48.35	10.23	0.53
20140513@605.asc	S7	Area 11	10	-12.7	17.8	0.3	20140404@273.asc	-3.4	1.1	3	0.208	38.08	49.52	10.02	2.37
20140513@604.asc	S7	Area 11	10	-9.1	21.6	0.3	20140404@274.asc	-0.3	1.1	4	0.160	42.72	48.32	8.16	0.80
20140513@586.asc	S7	Area 11	10	-9.5	21.1	0.2	20140404@279.asc	0.2	1.2	4	0.193	39.05	49.75	9.32	1.88
20140513@585.asc	S7	Area 11	10	-9.9	20.7	0.2	20140404@279.asc	0.2	1.2	4	0.193	39.05	49.75	9.32	1.88
20140513@591.asc	S7	Area 11	10	-8.2	22.5	0.4	20140404@286.asc	-0.4	1.2	4	0.141	41.97	50.71	6.88	0.44
20140513@592.asc	S7	Area 11	10	-7.6	23.1	0.4	20140404@283.asc	-1.3	1.2	4	0.120	42.22	51.37	5.74	0.67
20140513@592.asc	S7	Area 11	10	-7.6	23.1	0.4	20140404@282.asc	-1.2	1.2	4	0.162	39.67	51.32	7.58	1.42
20140513@584.asc	S7	Area 11	10	-13.7	16.8	0.2	20140404@281.asc	-2.4	1.2	5	0.213	35.81	51.95	9.69	2.56
20140513@583.asc	S7	Area 11	10	-10.2	20.4	0.2	20140404@280.asc	-6.2	1.2	6	0.338	28.33	54.78	14.48	2.41
20140513@581.asc	S7	Area 11	10	-12.2	18.3	0.2	20140404@285.asc	-6.2	1.2	6	0.390	24.87	56.19	15.95	2.98
20140513@594.asc	S7	Area 11	10	-12.7	17.8	0.4	20140404@285.asc	-6.2	1.2	6	0.390	24.87	56.19	15.95	2.98
20140513@582.asc	S7	Area 11	10	-13.5	17.0	0.2	20140404@284.asc	-7.1	1.2	6	0.483	20.93	55.43	19.50	4.14
20140513@593.asc	S7	Area 11	10	-13.8	16.7	0.4	20140404@284.asc	-7.1	1.2	6	0.483	20.93	55.43	19.50	4.14
20140107@158.asc	S2	Area 4	10	-10.9	19.7	0.5	20140404@243.asc	-1.0	0.6	2	0.182	39.07	51.75	8.71	0.47
20140107@155.asc	S2	Area 4	10	-11.0	19.6	0.5	20140404@244.asc	-1.5	0.6	4	0.184	39.41	50.79	8.90	0.90
20140107@156.asc	S2	Area 4	10	-10.4	20.2	0.5	20140404@245.asc	-0.9	0.6	4	0.156	39.95	52.03	7.38	0.64
20140107@157.asc	S2	Area 4	10	-14.1	16.4	0.5	20140404@246.asc	-5.4	0.6	5	0.251	34.37	50.83	11.54	3.27
20140107@164.asc	S2	Area 4	10	-8.5	22.1	0.3	20140404@249.asc	-5.7	0.6	6?	0.294	32.24	53.33	13.40	1.02
20140107@163.asc	S2	Area 4	10	-13.2	17.3	0.3	20140404@247.asc	-7.3	0.6	6	0.430	22.49	57.42	16.73	3.36
20140107@165.asc	S2	Area 4	10	-13.5	17.0	0.3	20140404@248.asc	-8.3	0.6	6	0.412	23.51	57.14	16.32	3.04
20140224@367.asc	S4	Area 2	3	-13.4	17.1	1.0	20140404@256.asc	-8.6	1.1	6	0.413	24.16	55.98	16.97	2.89
20140224@368.asc	S4	Area 2	3	-11.7	18.8	1.0	20140404@257.asc	-6.5	1.1	6	0.376	26.47	55.41	15.95	2.17
20140107@144.asc	S2	Area 2	10	-11.9	18.7	0.5	20140404@257.asc	-6.5	1.1	6	0.376	26.47	55.41	15.95	2.17
20140107@145.asc	S2	Area 2	10	-12.2	18.4	0.5	20140404@257.asc	-6.5	1.1	6	0.376	26.47	55.41	15.95	2.17
20140224@371.asc	S4	Area 2	3	-14.1	16.4	1.0	20140404@256.asc	-8.6	1.1	6	0.413	24.16	55.98	16.97	2.89
20140107@143.asc	S2	Area 2	10	-14.2	16.3	0.5	20140404@259.asc	-5.9	1.1	5	0.260	34.84	49.53	12.23	3.41
20140107@142.asc	S2	Area 2	10	-14.4	16.0	0.5	20140404@259.asc	-5.9	1.1	5	0.260	34.84	49.53	12.23	3.41
20140107@141.asc	S2	Area 2	10	-10.2	20.4	0.5	20140404@258.asc	-0.8	1.1	4	0.163	41.17	50.27	7.98	0.58
20140107@141.asc	S2	Area 2	10	-10.2	20.4	0.5	20140404@260.asc	-1.9	1.1	4	0.163	41.17	50.27	7.98	0.58
20140107@140.asc	S2	Area 2	10	-11.0	19.6	0.5	20140404@261.asc	-2.6	1.1	4	0.197	39.10	50.62	9.63	0.65
20140107@139.asc	S2	Area 2	10	-10.5	20.1	0.5	-	-	-	3	0.239	33.73	51.53	10.59	4.15
20140224@348.asc	S4	Area 10	3	-6.2	24.6	0.6	20140404@231.asc	0.9	0.7	4	0.125	41.55	51.93	5.86	0.66
20140224@338.asc	S4	Area 10	3	-5.5	25.2	0.9	20140404@231.asc	0.9	0.7	4	0.125	41.55	51.93	5.86	0.66
20140224@347.asc	S4	Area 10	3	-6.8	23.9	0.6	20140404@231.asc	0.9	0.7	4	0.125	41.55	51.93	5.86	0.66
20140107@175.asc	S2	Area 10	10	-6.9	23.8	0.2	20140404@232.asc	0.6	0.7	4	0.125	41.55	51.93	5.86	0.66
20140107@177.asc	S2	Area 10	10	-6.9	23.8	0.2	20140404@238.asc	0.7	0.7	4	0.125	41.55	51.93	5.86	0.66
20140107@177.asc	S2	Area 10	10	-6.9	23.8	0.2	20140404@233.asc	-0.4	0.7	4	0.125	41.55	51.93	5.86	0.66

20140224@339.asc	S4	Area 10	3	-8.5	22.2	0.9	20140404@235.asc	-4.8	0.7	6	0.352	28.59	53.98	15.49	1.94
20140107@176.asc	S2	Area 10	10	-12.2	18.3	0.2	20140404@235.asc	-4.8	0.7	6	**0.352**	28.59	53.98	15.49	1.94
20140107@178.asc	S2	Area 10	10	-12.5	18.0	0.2	20140404@235.asc	-4.8	0.7	6	**0.352**	28.59	53.98	15.49	1.94
20140224@335.asc	S4	Area 10	3	-9.9	20.7	0.9	20140404@234.asc	-7.2	0.7	6	0.401	24.98	55.46	16.66	2.90
20140224@336.asc	S4	Area 10	3	-11.2	19.4	0.9	20140404@234.asc	-7.2	0.7	6	0.401	24.98	55.46	16.66	2.90
20140224@349.asc	S4	Area 10	3	-12.2	18.3	0.6	20140404@234.asc	-7.2	0.7	6	0.401	24.98	55.46	16.66	2.90
20140224@337.asc	S4	Area 10	3	-12.3	18.3	0.9	20140404@234.asc	-7.2	0.7	6	0.401	24.98	55.46	16.66	2.90
20140224@340.asc	S4	Area 10	3	-13.1	17.4	0.9	20140404@237.asc	-7.7	0.7	6	0.406	24.71	55.48	16.83	2.97
20140224@345.asc	S4	Area 10	3	-13.6	16.9	0.6	20140404@237.asc	-7.7	0.7	6	0.406	24.71	55.48	16.83	2.97
20140224@346.asc	S4	Area 10	3	-13.6	16.9	0.6	20140404@236.asc	-7.9	0.7	6	0.287	41.04	55.28	14.99	2.30
20140107@199.asc	S2	Area 1	10	-10.1	20.5	0.5	-	-	-	4	0.161	40.83	50.71	7.83	0.63
20140107@200.asc	S2	Area 1	10	-11.2	19.4	0.5	-	-	-	3?	0.221	35.82	52.46	10.14	1.58
20140107@198.asc	S2	Area 1	10	-13.8	16.6	0.5	-	-	-	5	0.228	34.69	52.30	10.18	2.83
20140107@197.asc	S2	Area 1	10	-12.1	18.4	0.5	-	-	-	6	0.364	26.01	56.82	14.85	2.33
20140107@196.asc	S2	Area 1	10	-14.1	16.4	0.5	-	-	-	6	0.422	23.06	56.69	16.78	3.46
20140107@195.asc	S2	Area 1	10	-12.8	17.7	0.5	-	-	-	6	0.394	24.50	56.84	15.78	2.88
20140107@190.asc	S2	Area 1	10	-10.8	19.7	0.5	-	-	-	2	0.228	35.48	51.91	10.43	2.18
20140107@191.asc	S2	Area 1	10	-11.1	19.4	0.5	-	-	-	2	0.228	35.48	51.91	10.43	2.18
20140107@192.asc	S2	Area 1	10	-9.4	21.2	0.5	-	-	-	4	0.169	39.75	51.40	8.11	0.74
20140107@193.asc	S2	Area 1	10	-12.3	18.2	0.5	-	-	-	5	0.364	25.91	57.13	14.80	2.16
20140107@194.asc	S2	Area 1	10	-11.4	19.1	0.5	-	-	-	5	0.319	29.09	54.66	13.53	2.72
-	-	Area 12	-	-	-	-	20140405@415.asc	-0.9	1.0	1	0.196	37.37	51.88	9.02	1.73
-	-	Area 12	-	-	-	-	20140405@416.asc	-2.0	1.0	1	0.236	35.64	51.20	11.02	2.15
-	-	Area 12	-	-	-	-	20140405@417.asc	-1.6	1.0	1	0.242	37.21	50.30	11.82	0.66
-	-	Area 12	-	-	-	-	20140405@418.asc	-1.3	1.0	1	0.198	39.68	49.92	9.79	0.61
-	-	Area 12	-	-	-	-	20140405@419.asc	-1.6	1.0	1	0.252	36.21	49.38	12.19	2.22
-	-	Area 12	-	-	-	-	20140405@420.asc	-3.0	1.0	1	0.174	39.52	51.61	8.31	0.56
-	-	Area 12	-	-	-	-	20140405@421.asc	-0.7	1.0	1	0.209	38.96	50.02	10.31	0.71
-	-	Area 12	-	-	-	-	20140405@422.asc	-0.8	1.0	1	0.174	39.52	51.61	8.31	0.56
-	-	Area 12	-	-	-	-	20140405@427.asc	-8.1	0.8	6	0.427	23.77	55.57	17.64	3.03
-	-	Area 12	-	-	-	-	20140405@428.asc	-5.8	0.8	6	0.348	28.53	54.37	15.25	1.85
-	-	Area 12	-	-	-	-	20140405@429.asc	-4.7	0.8	5	0.236	35.48	50.59	10.96	2.97
-	-	Area 12	-	-	-	-	20140405@430.asc	0.5	0.8	4	0.168	40.34	50.95	8.14	0.58
-	-	Area 12	-	-	-	-	20140405@431.asc	-0.5	0.8	4	0.129	43.74	49.17	6.48	0.62
-	-	Area 12	-	-	-	-	20140405@432.asc	-0.4	0.8	2	0.210	38.07	51.17	10.13	0.62
-	-	Area 12	-	-	-	-	20140405@433.asc	-0.1	0.8	2	0.178	40.76	49.92	8.86	0.46
-	-	Area 12	-	-	-	-	20140405@434.asc	-2.3	0.8	1	0.257	35.14	50.59	12.12	2.15

Table 2. Isotopic composition ($\delta^{13}C$ and $\delta^{18}O$) of carbonate cements in the Eau Claire shale (C13637, depth = 3597.5 ft)

Session specific sample I.D.	SIMS session	Sample region i.d.	Spot-size (μm)	$\delta^{18}O$‰ PDB	$\delta^{18}O$‰ V-SMOW	2SD	$\delta^{13}C$‰ PDB	2SD	Zone	Fe#	$MgCO_3$ (mol.%)	$CaCO_3$ (mol.%)	$FeCO_3$ (mol.%)	$MnCO_3$ (mol.%)
20140212@156.asc	S3	A1 R1	10	-4.2	26.6	0.2	-	-	Z0	0.007	41.91	57.74	0.31	0.04
20140212@163.asc	S3	A2 R2	10	-4.4	26.3	0.2	-	-	Z0	0.007	41.91	57.74	0.31	0.04
20140212@171.asc	S3	A3 R3	10	-5.3	25.5	0.2	-	-	Z0	0.007	41.91	57.74	0.31	0.04
20140212@178.asc	S3	A4 R4a	10	-5.2	25.6	0.2	-	-	Z0	0.007	41.91	57.74	0.31	0.04
20140212@206.asc	S3	A6 R6	10	-4.6	26.1	0.4	-	-	Z0	0.007	41.91	57.74	0.31	0.04
20140405@443.asc	S5	An-1	6	-	-	-	4.2	0.8	Z0	0.007	41.65	58.00	0.31	0.04
20140405@444.asc	S5	An-1	6	-	-	-	3.1	0.8	Z0	0.007	41.65	58.00	0.31	0.04
20140405@455.asc	S5	An-2	6	-	-	-	2.6	0.7	Z0	0.007	41.65	58.00	0.31	0.04
20140405@491.asc	S5	A3	6	-	-	-	3.9	0.8	Z0	0.007	41.65	58.00	0.31	0.04
		Average of Zone 0		**-4.7**	**26.0**	**-**	**3.5**	**-**	**-**	**0.007**	**41.79**	**57.86**	**0.31**	**0.04**
		2SD		0.9	1.0	-	1.5	-	-	0.000	0.27	0.27	0.00	0.00
20140212@164.asc	S3	A2 R2	10	-5.9	24.9	0.2	-	-	Z1a	0.225	31.40	58.90	9.10	0.50
20140212@166.asc	S3	A2 R2	10	-6.2	24.5	0.2	-	-	Z1a	0.225	31.40	58.90	9.10	0.50
20140405@447.asc	S5	An-1	6	-	-	-	9.3	0.8	Z1a	0.218	31.13	59.65	8.69	0.53
20140405@448.asc	S5	An-1	6	-	-	-	9.7	0.8	Z1a	0.196	33.54	57.81	8.19	0.46
20140405@456.asc	S5	An-2	6	-	-	-	8.7	0.7	Z1a	0.168	36.00	56.33	7.26	0.41
20140405@462.asc	S5	An-3	6	-	-	-	9.6	0.7	Z1a	0.236	31.35	58.38	9.66	0.61
20140405@471.asc	S5	A5 exp	6	-	-	-	11.3	0.7	Z1a	0.236	31.35	58.38	9.66	0.61
20140405@472.asc	S5	A5 exp	6	-	-	-	12.5	0.7	Z1a	0.236	31.35	58.38	9.66	0.61
20140405@492.asc	S5	A3	6	-	-	-	7.4	0.8	Z1a	0.182	34.73	57.10	7.75	0.42
20140405@508.asc	S5	A5 exp1	6	-	-	-	8.1	0.9	Z1a	0.217	31.44	59.33	8.75	0.48
		Average of Zone 1a		**-6.0**	**24.7**	**-**	**9.6**	**-**	**-**	**0.214**	**32.37**	**58.32**	**8.78**	**0.51**
		2SD		0.5	0.5	-	3.3	-	-	0.048	3.50	2.02	1.67	0.15
20140212@172.asc	S3	A3 R3	10	-5.4	25.4	0.2	-	-	Z1b	0.167	34.46	57.77	6.89	0.88
20140212@179.asc	S3	A4 R4a	10	-5.0	25.8	0.2	-	-	Z1b	0.099	37.18	58.32	4.09	0.41
20140212@180.asc	S3	A4 R4a	10	-5.6	25.1	0.2	-	-	Z1b	0.120	34.71	59.79	4.72	0.78
20140212@183.asc	S3	A4 R4a	10	-5.7	25.0	0.2	-	-	Z1b	0.121	35.24	59.45	4.88	0.43
20140212@198.asc	S3	A4 R4b	10	-5.7	25.1	0.4	-	-	Z1b	0.127	35.47	58.90	5.15	0.49
20140212@461.asc	S3	A1 R1	10	-5.9	24.9	0.2	-	-	Z1b	0.092	38.65	57.02	3.90	0.43
20140212@471.asc	S3	A5 SR1	10	-5.6	25.2	0.2	-	-	Z1b	0.114	36.27	58.63	4.68	0.42
20140405@467.asc	S5	An-3	6	-	-	-	10.4	0.7	Z1b	0.127	35.05	59.38	5.10	0.47
20140405@468.asc	S5	An-3	6	-	-	-	11.6	0.7	Z1b	0.127	35.05	59.38	5.10	0.47
20140405@482.asc	S5	A5 exp	6	-	-	-	13.1	0.8	Z1b	0.123	36.55	57.95	5.13	0.36
20140405@486.asc	S5	A5 exp	6	-	-	-	14.3	0.8	Z1b	0.123	36.55	57.95	5.13	0.36

20140405@493.asc	S5	A3	6	-	-	-	7.3	0.8	Z1b	0.137	35.06	58.92	5.56	0.46
20140405@516.asc	S5	A5 exp5	6	-	-	-	11.7	0.9	Z1b	0.107	38.10	56.84	4.58	0.49
20140405@517.asc	S5	A5 exp6	6	-	-	-	9.4	0.9	Z1b	0.132	35.46	58.48	5.42	0.64
20140405@518.asc	S5	A5 exp7	6	-	-	-	7.2	0.9	Z1b	0.141	35.97	57.10	5.90	1.03
		Average of Zone 1b		**-5.5**	**25.2**	**-**	**10.6**	**-**	**-**	**0.124**	**35.98**	**58.39**	**5.08**	**0.54**
			2SD	0.6	0.6	-	5.2	-	-	0.036	2.47	1.88	1.44	0.40
20140212@173.asc	S3	A3 R3	10	-8.0	22.6	0.2	-	-	Z2a	0.289	27.41	61.10	11.14	0.35
20140212@181.asc	S3	A4 R4a	10	-7.5	23.2	0.2	-	-	Z2a	0.253	30.93	59.08	9.52	0.47
20140405@445.asc	S5	An-1	6	-	-	-	6.6	0.8	Z2a	0.295	29.20	58.21	12.26	0.33
20140405@461.asc	S5	An-3	6	-	-	-	5.9	0.7	Z2a	0.231	32.05	57.84	9.62	0.50
20140405@469.asc	S5	An-3	6	-	-	-	7.2	0.7	Z2a	0.299	28.74	58.51	12.26	0.50
20140405@509.asc	S5	A5 exp2	6	-	-	-	7.8	0.9	Z2a	0.290	29.78	57.62	12.18	0.42
20140405@519.asc	S5	A5 exp2	6	-	-	-	9.7	0.9	Z2a	0.272	28.73	60.24	10.73	0.31
		Average of Zone 2a		**-7.7**	**22.9**	**-**	**7.4**	**-**	**-**	**0.276**	**29.55**	**58.94**	**11.10**	**0.41**
			2SD	0.8	0.8	-	2.9	-	-	0.050	3.08	2.59	2.41	0.16
20140212@158.asc	S3	A1 R1	10	-8.2	22.4	0.2	-	-	Z2b	0.245	31.11	58.47	10.12	0.31
20140212@174.asc	S3	A3 R3	10	-8.0	22.6	0.2	-	-	Z2b	0.245	31.79	57.48	10.32	0.41
20140212@182.asc	S3	A4 R4a	10	-8.2	22.4	0.2	-	-	Z2b	0.238	32.13	57.38	10.05	0.44
20140212@184.asc	S3	A4 R4a	10	-8.0	22.7	0.2	-	-	Z2b	0.232	29.94	60.58	9.03	0.45
20140212@210.asc	S3	A6 R6	10	-7.2	23.4	0.4	-	-	Z2b	0.270	30.56	57.62	11.30	0.52
20140212@216.asc	S3	A5 R5	10	-8.5	22.2	0.4	-	-	Z2b	0.237	31.20	58.67	9.70	0.43
20140212@462.asc	S3	A1 R1	10	-8.9	21.7	0.2	-	-	Z2b	0.253	32.66	55.73	11.00	0.60
20140212@473.asc	S3	A5 SR1	10	-7.8	22.8	0.2	-	-	Z2b	0.232	33.21	56.51	10.04	0.24
20140212@479.asc	S3	A5 SR1	10	-8.1	22.6	0.3	-	-	Z2b	0.229	32.44	57.34	9.64	0.58
20140405@446.asc	S5	An-1	6	-	-	-	7.1	0.8	Z2b	0.222	34.05	55.94	9.69	0.32
20140405@473.asc	S5	A5 exp	6	-	-	-	9.2	0.7	Z2b	0.243	32.82	56.26	10.53	0.39
20140405@483.asc	S5	A5 exp	6	-	-	-	10.2	0.8	Z2b	0.238	32.62	56.69	10.17	0.52
20140405@484.asc	S5	A5 exp	6	-	-	-	10.8	0.8	Z2b	0.286	30.98	56.13	12.42	0.47
		Average of Zone 2b		**-8.1**	**22.5**	**-**	**9.3**	**-**	**-**	**0.244**	**31.96**	**57.29**	**10.31**	**0.44**
			2SD	0.9	0.9	-	3.3	-	-	0.035	2.32	2.70	1.73	0.21
20140212@175.asc	S3	A3 R3	10	-7.6	23.1	0.2	-	-	Z3	0.094	40.12	55.55	4.17	0.15
20140212@191.asc	S3	A4 R4a	10	-7.6	23.1	0.4	-	-	Z3	0.109	38.69	56.38	4.74	0.19
20140212@193.asc	S3	A4 R4b	10	-8.2	22.5	0.4	-	-	Z3	0.089	39.90	56.00	3.90	0.20
20140212@195.asc	S3	A4 R4b	10	-6.4	24.3	0.4	-	-	Z3	0.081	39.15	57.21	3.42	0.22
20140212@196.asc	S3	A4 R4b	10	-7.9	22.8	0.4	-	-	Z3	0.081	39.15	57.21	3.42	0.22
20140212@197.asc	S3	A4 R4b	10	-6.5	24.2	0.4	-	-	Z3	0.081	39.15	57.21	3.42	0.22
20140212@207.asc	S3	A6 R6	10	-7.0	23.6	0.4	-	-	Z3	0.089	39.90	56.00	3.90	0.20

20140212@209.asc	S3	A6 R6	10	-7.7	23.0	0.4	-	-	Z3	0.096	39.95	55.56	4.27	0.22
20140212@472.asc	S3	A5 SR1	10	-7.8	22.9	0.2	-	-	Z3	0.083	39.53	56.74	3.59	0.15
20140212@478.asc	S3	A5 SR1	10	-6.8	23.8	0.3	-	-	Z3	0.094	42.07	53.39	4.36	0.18
20140212@464.asc	S3	A1 R1	10	-8.8	21.9	0.2	-	-	Z3	0.124	36.92	57.56	5.22	0.29
20140405@449.asc	S5	An-1	6	-	-	-	6.6	0.8	Z3	0.061	40.39	56.78	2.67	0.17
20140405@450.asc	S5	An-1	6	-	-	-	5.5	0.8	Z3	0.050	40.63	57.01	2.14	0.22
20140405@474.asc	S5	A5 exp	6	-	-	-	9.0	0.7	Z3	0.128	38.70	55.35	5.68	0.26
20140405@494.asc	S5	A3	6	-	-	-	5.0	0.8	Z3	0.052	42.61	54.83	2.35	0.20
20140405@495.asc	S5	A3	6	-	-	-	5.8	0.8	Z3	0.052	42.61	54.83	2.35	0.20
20140405@498.asc	S5	An-1	6	-	-	-	7.1	0.8	Z3	0.085	41.60	54.39	3.88	0.14
20140405@515.asc	S5	A5 exp4	6	-	-	-	8.6	0.9	Z3	0.125	38.72	55.52	5.52	0.25
20140405@521.asc	S5	A5 exp10	6	-	-	-	8.3	0.9	Z3	0.106	39.20	55.93	4.66	0.20
20140405@522.asc	S5	A5 exp11	6	-	-	-	7.4	0.9	Z3	0.109	39.01	55.98	4.77	0.23
		Average of Zone 3		**-7.5**	**23.2**	**-**	**7.0**	**-**	**-**	**0.089**	**39.90**	**55.97**	**3.92**	**0.21**
			2SD	1.4	1.5	-	2.9	-	-	0.047	2.88	2.17	2.06	0.07

Table 3. Isotopic composition ($\delta^{18}O$) of quartz-overgrowths in the upper Mt. Simon Sandstone (ADM Verification Well #1; depth = 5513.2 ft)

Session specific sample I.D.	SIMS session i.d.	Sample region i.d.	Spot-size (µm)	$\delta^{18}O$‰ (VSMOW)	± (2SD)	QO Zone
20140224@372.asc	S4	Area 2	3	22.4	1.0	1
20140224@370.asc	S4	Area 2	3	23.6	1.0	1
20140224@357.asc	S4	Area 10	3	23.7	1.0	1
20140224@360.asc	S4	Area 10	3	22.7	1.0	1
20140224@359.asc	S4	Area 10	3	23.4	0.8	1
20140107@211.asc	S2	Area 1	10	28.5	0.5	2
20140107@210.asc	S2	Area 1	10	27.7	0.5	2
20140107@153.asc	S2	Area 2	10	27.4	0.5	2
20140107@179.asc	S2	Area 10	10	27.3	0.2	2
20140107@168.asc	S2	Area 4	10	27.5	0.3	2
20140513@610.asc	S7	Area 11	10	25.7	0.3	2
20140107@208.asc	S2	Area 1	10	21.5	0.5	3
20140107@166.asc	S2	Area 4	10	22.2	0.3	3
20140107@170.asc	S2	Area 4	10	23.2	0.3	3
20140513@621.asc	S7	Area 11	10	21.9	0.3	3
20140107@207.asc	S2	Area 1	10	21.1	0.5	4
20140107@214.asc	S2	Area 1	10	21.0	0.5	4
20140107@212.asc	S2	Area 1	10	22.0	0.5	4
20140107@213.asc	S2	Area 1	10	20.8	0.5	4
20140107@154.asc	S2	Area 2	10	21.2	0.5	4
20140224@369.asc	S4	Area 2	3	21.4	1.0	4
20140224@355.asc	S4	Area 10	3	21.3	0.8	4
20140224@356.asc	S4	Area 10	3	21.8	0.8	4
20140107@180.asc	S2	Area 10	10	21.3	0.2	4
20140513@608.asc	S7	Area 11	10	21.7	0.3	4
20140513@612.asc	S7	Area 11	10	22.0	0.3	4

Table 4. Predicted C-isotope composition of sequestration-related carbonate cements at the Illinois Basin Decatur Project site.

Carb. mineral - CO_2 (g) eq. fractionation relationships	**Calibrated Range (°C)**	**$\delta^{13}C$ CO_2 (‰, VPDB)**	**Reservoir T(°C)**	**Predicted $\delta^{13}C_{carbonate}$ (‰, VPDB)**
[a] $10^3 \ln\alpha(\text{siderite-}CO_2) = 2.53\ (10^6 / T^2) - 20.20$	25-197°C	-10	50	**-6**
[b] $10^3 \ln\alpha(\text{dolomite-}CO_2) = 1.637\ (10^6 / T^2) - 7.29$	100-250°C	-10	50	**-2**
[c] $10^3 \ln\alpha(\text{calcite-}CO_2) = 1.648\ (10^6 / T^2) - 8.02$	25-200°C (theoretical)	-10	50	**-2**

[a] Jimenez-Lopez and Romanek (2004): Using the results presented in their Fig. 9a, specifically the linear trend that incorporates their experimental results at 25°C and those of Carothers et al. (1988) out to 197°C, corrected for T and pH.

[b] Eq. 6 of Horita (2014) recast as $1000\ln\alpha(\text{dolomite-}CO_2)$; originally presented as $1000\ln\alpha(CO_2\text{-dolomite})$

[c] Chacko et al. (1991): Theoretical values from Table 7 between 25 and 200°C. Recast as $1000\ln\alpha(\text{calcite-}CO_2)$; originally presented as $1000\ln\alpha(CO_2\text{-calcite})$

Fig. 1

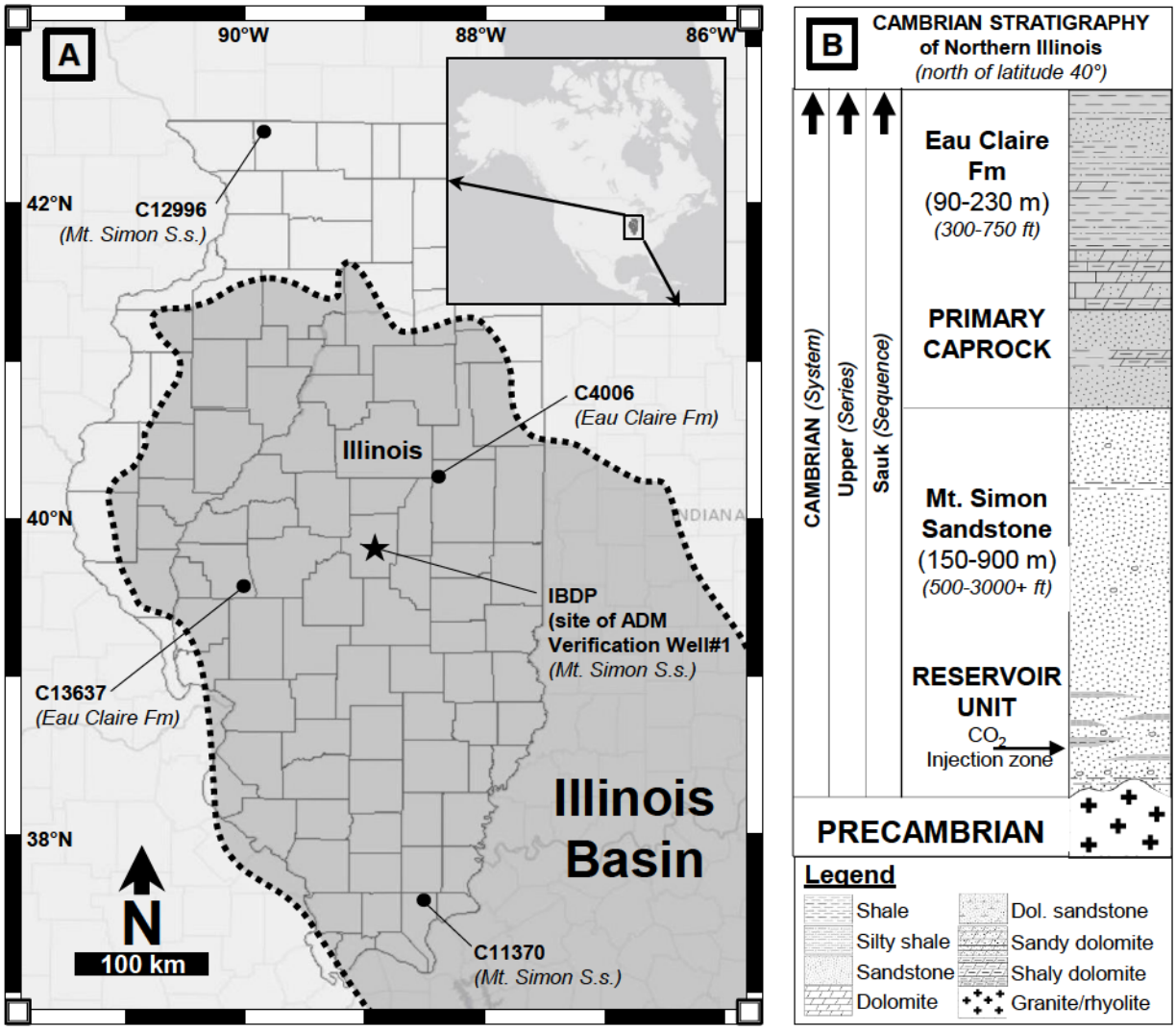
A
90°W
88°W
86°W
42°N
40°N
38°N
C12996
(Mt. Simon S.s.)
C4006
(Eau Claire Fm)
Illinois
IBDP
(site of ADM
Verification Well#1
(Mt. Simon S.s.)
C13637
(Eau Claire Fm)
Illinois
Basin
N
100 km
C11370
(Mt. Simon S.s.)
B
CAMBRIAN STRATIGRAPHY
of Northern Illinois
(north of latitude 40°)
CAMBRIAN (System)
Upper (Series)
Sauk (Sequence)
Eau Claire
Fm
(90-230 m)
(300-750 ft)
PRIMARY
CAPROCK
Mt. Simon
Sandstone
(150-900 m)
(500-3000+ ft)
RESERVOIR
UNIT
CO2
Injection zone
PRECAMBRIAN
Legend
Shale
Silty shale
Sandstone
Dolomite
Dol. sandstone
Sandy dolomite
Shaly dolomite
Granite/rhyolite

Fig. 2

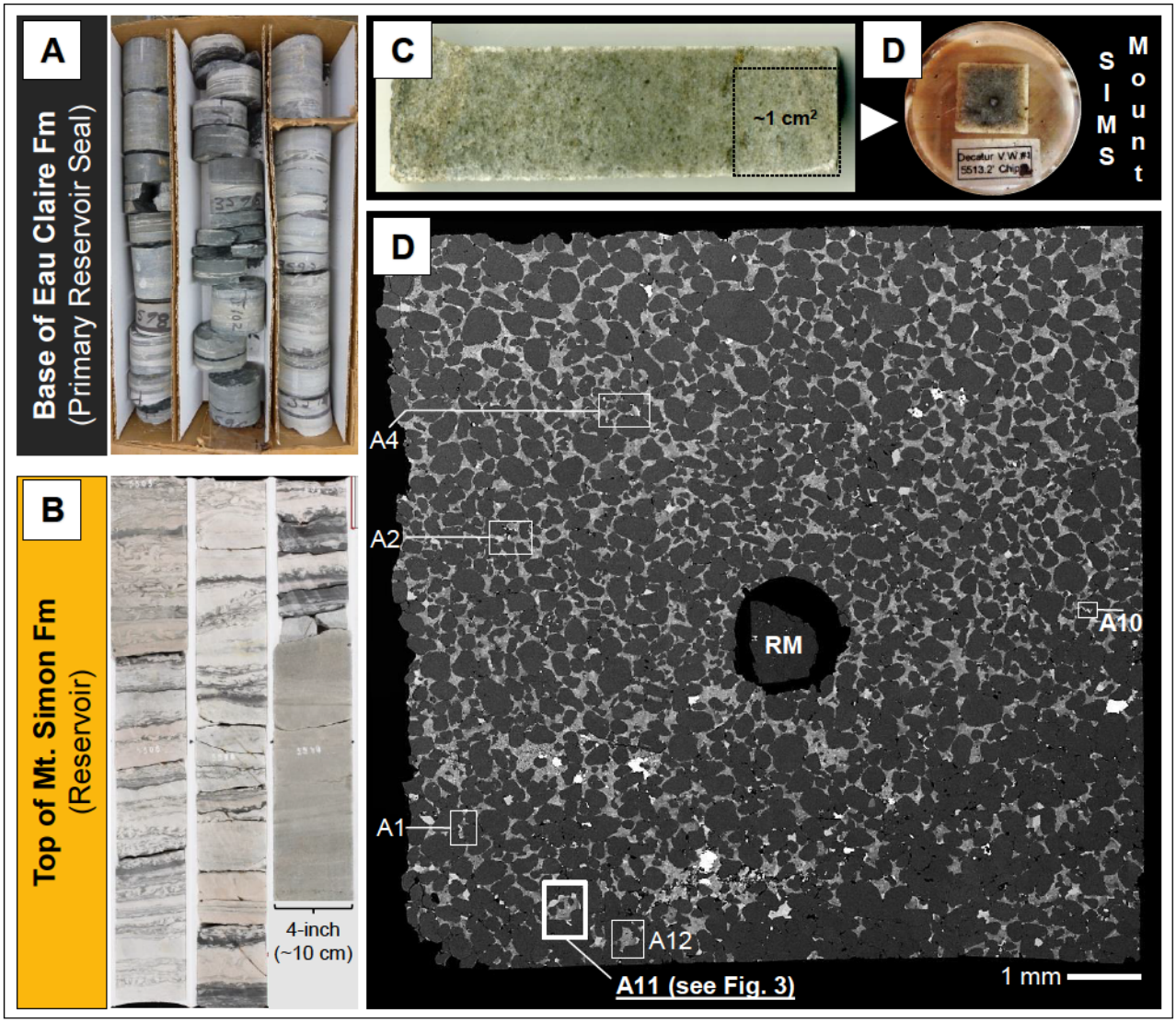
A
Base of Eau Claire Fm
(Primary Reservoir Seal)
B
Top of Mt. Simon Fm
(Reservoir)
4-inch
(~10 cm)
C
~1 cm²
D
SIMS Mount
Decatur V.W.#1
5513.2' Chip
D
A4
A2
RM
A10
A1
A12
A11 (see Fig. 3)
1 mm

Fig. 3

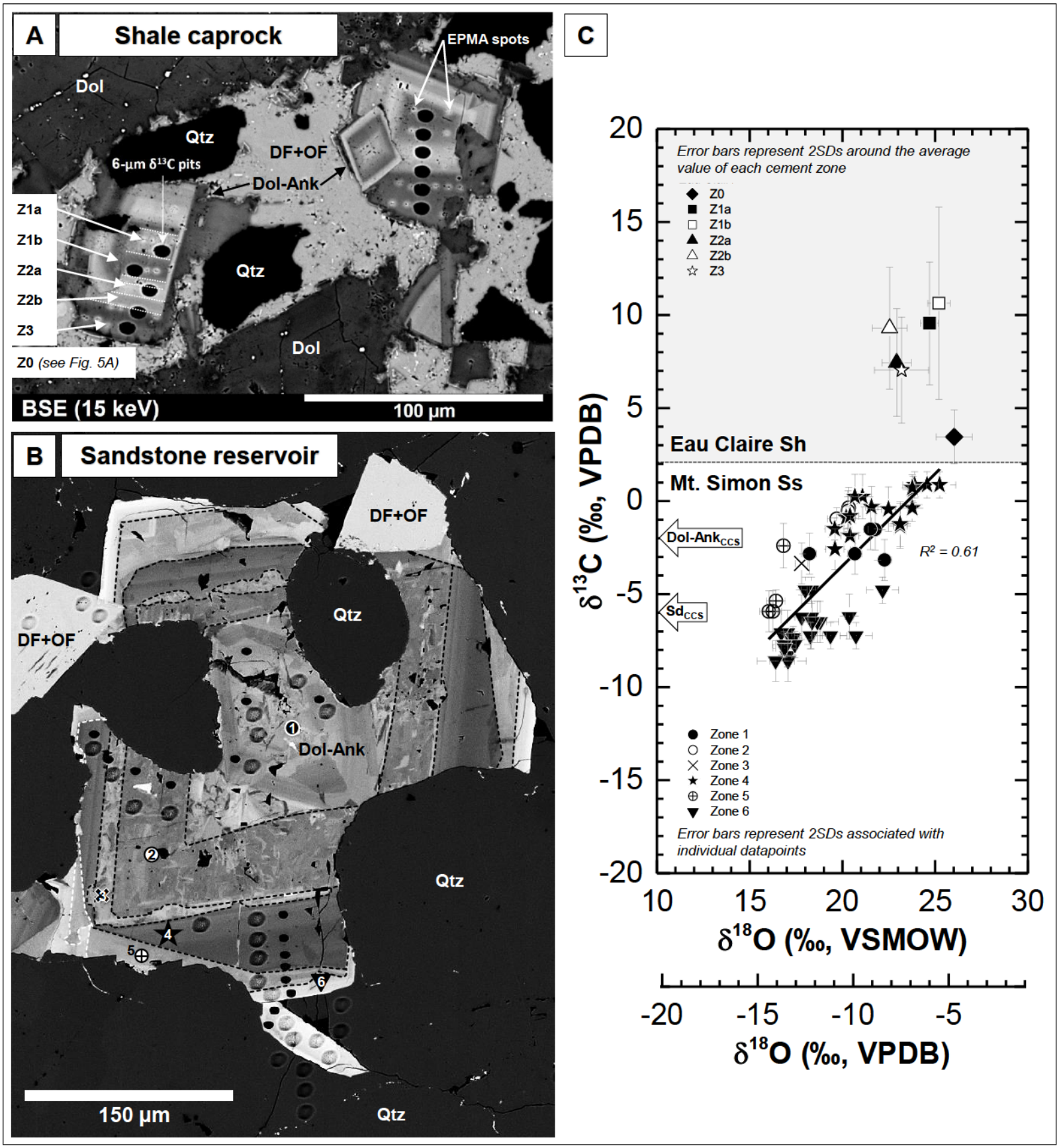
A
Shale caprock
EPMA spots
Dol
Qtz
6-µm δ13C pits
DF+OF
Dol-Ank
Z1a
Z1b
Z2a
Z2b
Z3
Qtz
Dol
Z0 (see Fig. 5A)
BSE (15 keV)
100 µm
B
Sandstone reservoir
DF+OF
Qtz
DF+OF
Dol-Ank
Qtz
Qtz
150 µm
C
Error bars represent 2SDs around the average value of each cement zone
Z0
Z1a
Z1b
Z2a
Z2b
Z3
Eau Claire Sh
Mt. Simon Ss
Dol-Ankccs
Sdccs
R² = 0.61
Zone 1
Zone 2
Zone 3
Zone 4
Zone 5
Zone 6
Error bars represent 2SDs associated with individual datapoints
δ13C (‰, VPDB)
δ18O (‰, VSMOW)
δ18O (‰, VPDB)

Fig. 4

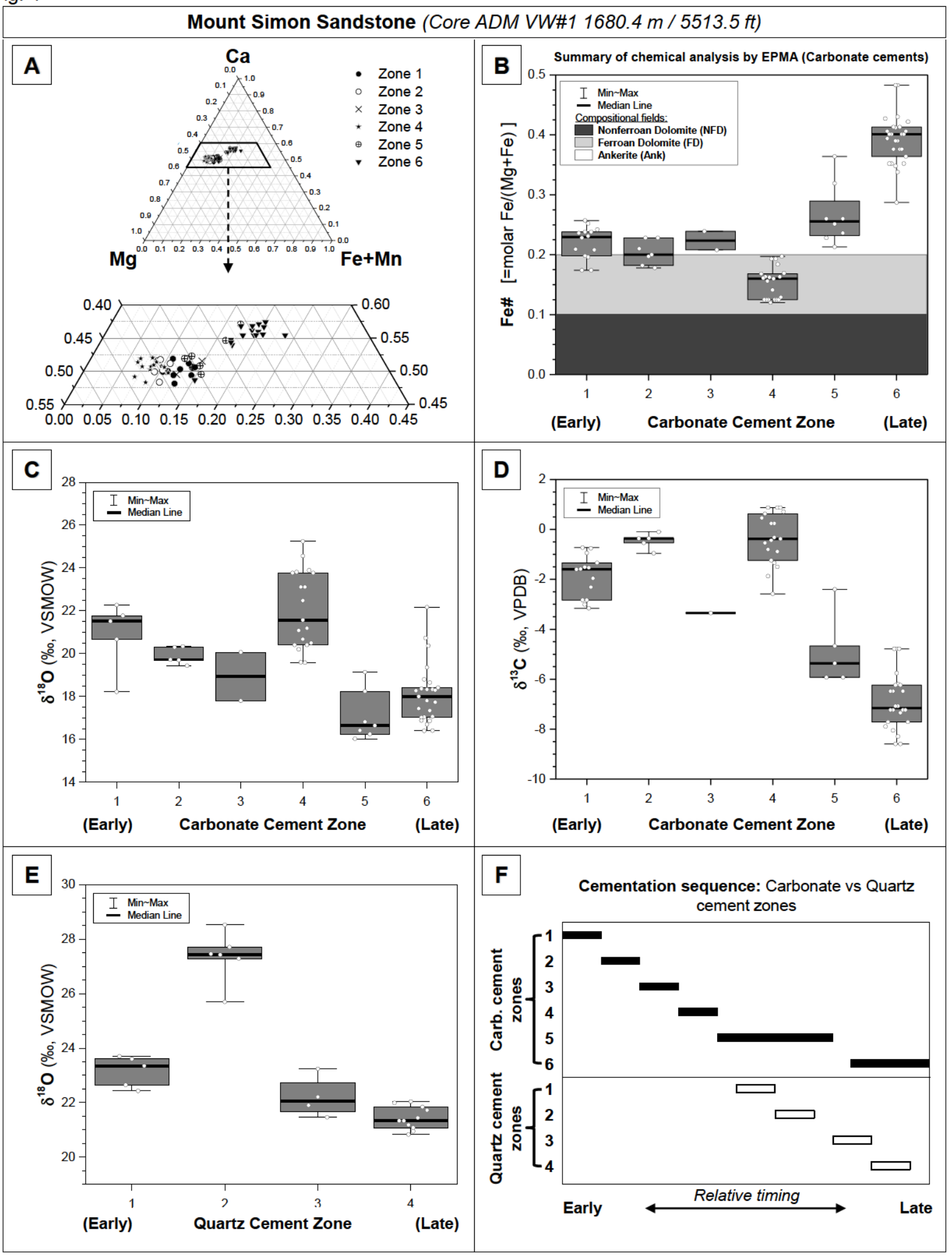
Mount Simon Sandstone (Core ADM VW#1 1680.4 m / 5513.5 ft)
A
Ca
Mg
Fe+Mn
Zone 1
Zone 2
Zone 3
Zone 4
Zone 5
Zone 6
B
Summary of chemical analysis by EPMA (Carbonate cements)
Min~Max
Median Line
Compositional fields:
Nonferroan Dolomite (NFD)
Ferroan Dolomite (FD)
Ankerite (Ank)
Fe# [=molar Fe/(Mg+Fe)]
(Early)
Carbonate Cement Zone
(Late)
C
δ18O (‰, VSMOW)
Min~Max
Median Line
(Early)
Carbonate Cement Zone
(Late)
D
δ13C (‰, VPDB)
Min~Max
Median Line
(Early)
Carbonate Cement Zone
(Late)
E
δ18O (‰, VSMOW)
Min~Max
Median Line
(Early)
Quartz Cement Zone
(Late)
F
Cementation sequence: Carbonate vs Quartz cement zones
Carb. cement zones
Quartz cement zones
Relative timing
Early
Late

Fig. 5

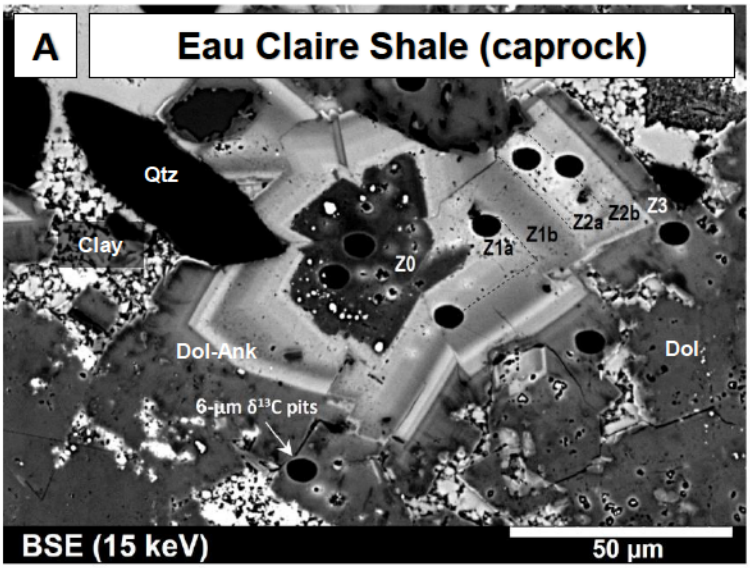
A
Eau Claire Shale (caprock)
Qtz
Clay
Z0
Z1a
Z1b
Z2a
Z2b
Z3
Dol-Ank
Dol
6-µm δ13C pits
BSE (15 keV)
50 µm

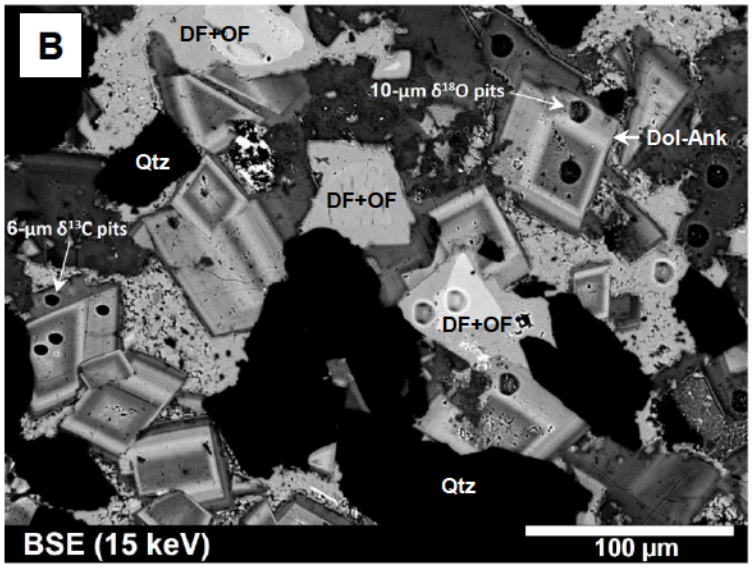
B
DF+OF
10-µm δ18O pits
Dol-Ank
Qtz
DF+OF
6-µm δ13C pits
DF+OF
Qtz
BSE (15 keV)
100 µm

Fig. 6

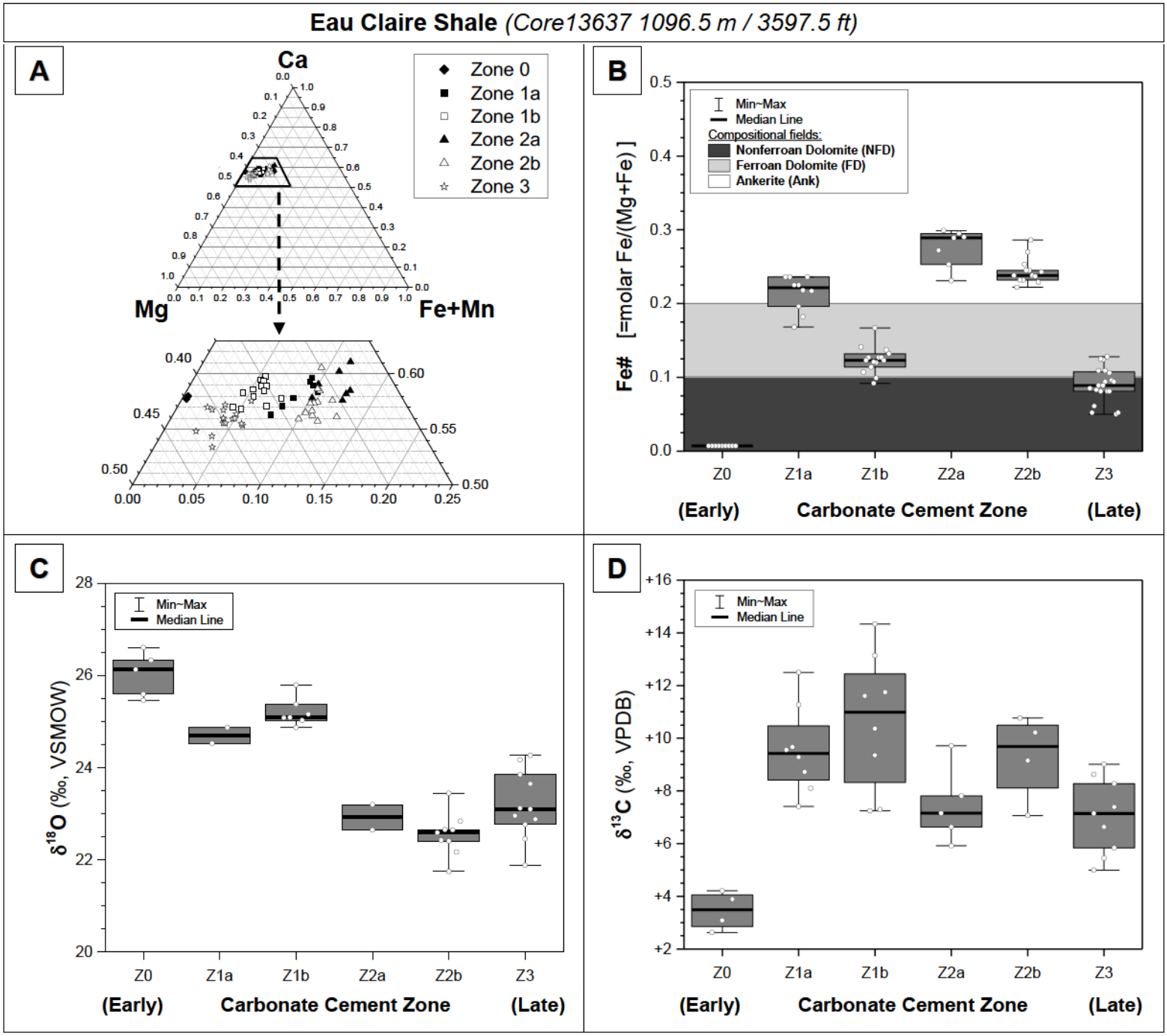
Eau Claire Shale (Core13637 1096.5 m / 3597.5 ft)
A
Ca
Mg
Fe+Mn
Zone 0
Zone 1a
Zone 1b
Zone 2a
Zone 2b
Zone 3
B
Fe# [=molar Fe/(Mg+Fe)]
Min~Max
Median Line
Compositional fields:
Nonferroan Dolomite (NFD)
Ferroan Dolomite (FD)
Ankerite (Ank)
Z0
Z1a
Z1b
Z2a
Z2b
Z3
(Early)
Carbonate Cement Zone
(Late)
C
δ18O (‰, VSMOW)
D
δ13C (‰, VPDB)

Fig. 7

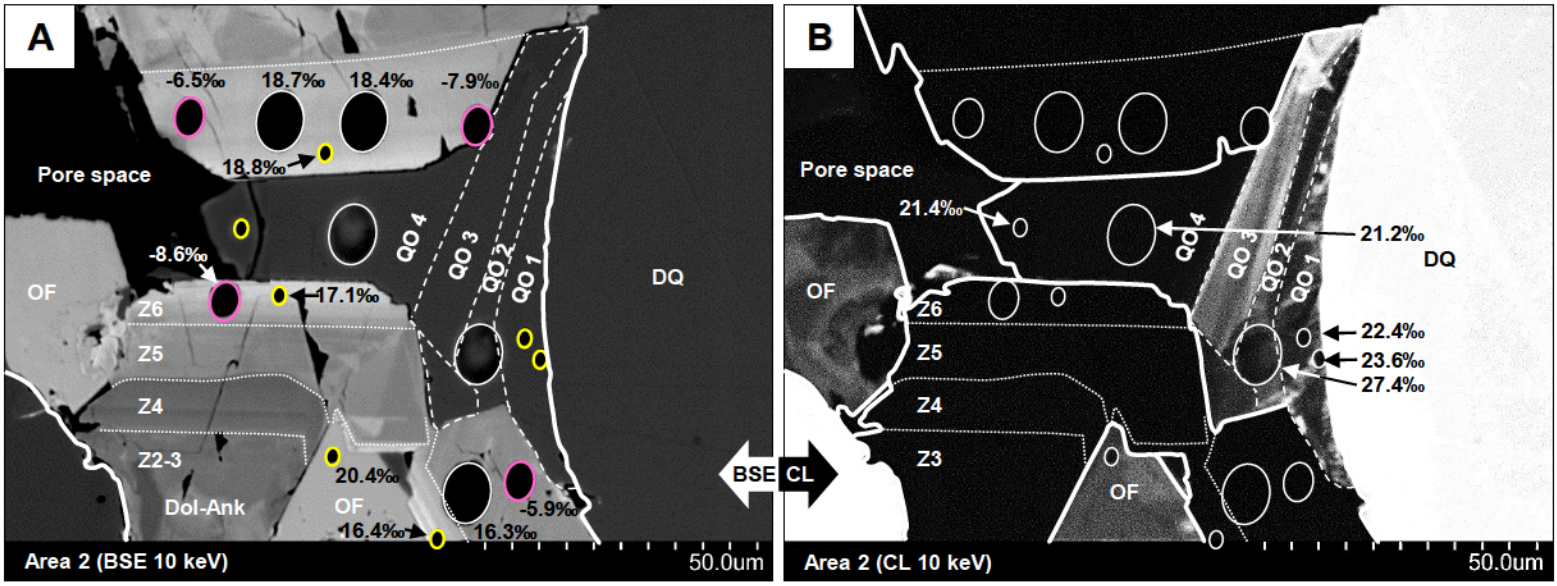

Legend

$\delta^{18}O$ 3-µm SIMS pits $\delta^{18}O$ 10-µm SIMS $\delta^{13}C$ 6-µm SIMS pits

QO 1-4 = Quartz-overgrowth zones; **DQ** = Detrital quartz grain; **Z 1-6** = Carbonate cement zones; **DF** = Detrital K-feldspar grain; **OF** = Overgrowth K-feldspar

SUPPLEMENTARY APPENDIX 5

A brief note on the possible origin of diagenetic carbonate cements in the Mount Simon-Eau Claire system

We offer the following possible explanation for the contrasting evolution of carbon isotope ratios in the upper Mt. Simon Sandstone and the Eau Claire shale.

Positive $\delta^{13}C$ values of dolomite-ankerite cements in the Eau Claire shale indicate that during sediment burial, conditions favorable to bacterial methanogenesis may have taken hold as microbial communities acted to decompose/recycle sedimentary organic matter (OM). Microbial OM recycling proceeds sequentially through several different characteristic stages, all of which produce CO_2 that is released into porewaters; these stages are the following: aerobic oxidation, followed by the reduction of nitrate (NO_3^{2-}), Fe and Mn-oxides and sulfate (SO_4^{2-}), and lastly fermentation (bacterial methanogenesis, up to a temperature of ~75°C; *e.g.,* Heese, 1999). Certain distinctive trends have been recognized with regards to the C-isotope composition of the CO_2 that is produced during these reactions (Irwin et al., 1977). The first three stages produce CO_2 (which may equilibrate with porewaters to form dissolved HCO_3^- and CO_3^{2-} ions) with $\delta^{13}C$ values that resemble that of the bulk organic matter (average of -25‰ VPDB; *e.g.,* Fig. 1 in Irwin et al., 1977). Thus, the $\delta^{13}C$ of carbon dissolved in porewaters tends towards -25‰ (VPDB; depending on volume of OM-derived CO_2 that is generated). Carbonate cements that precipitate during these stages take on negative $\delta^{13}C$ values. For example: if $\delta^{13}C$ of porewater CO_2 = -25‰, the $\delta^{13}C$ of dolomite will be -16.5‰ at 50°C and -21.5‰ at 120°C (Horita, 2014). In contrast, bacterial methanogenesis can proceed, *e.g.,* by consuming CO_2 (as an oxidizer; other reaction pathways discussed are reviewed by Whiticar, 1999), yielding methane gas (CH_4) with exceptionally negative $\delta^{13}C$ values (down to -110‰). The residual CO_2 reservoir thus becomes enriched in ^{13}C, acquiring $\delta^{13}C$ values that are higher than those of CH_4 by 40-100‰ (values may reach +15-20‰; *e.g.,* Fig. 1 in Irwin et al., 1977; Whiticar, 1999). Carbonate cements that precipitate during this stage of OM recycling may take on positive $\delta^{13}C$ values (depending on the extent to which the residual dissolved CO_2 pool is enriched in ^{13}C; *e.g.,* Heese, 1999, Whiticar, 1999). For example: if $\delta^{13}C$ of porewater CO_2 = +5‰, then the $\delta^{13}C$ value of dolomite will be +16.75‰ at 20°C, +13.5‰ at 50°C, and +8.5‰ at 120°C (Horita, 2014). At the maximum reconstructed burial depth of the examined Eau Claire shale bed (Fig. 1; ~2 km / 6500 ft; after Rowan et al., 2002), temperatures due to burial alone, excluding late hydrothermal heating associated with the genesis of regional Mississippi-Valley type ore deposits, are estimated at a maximum of ~80°C (Makowitz et al., 2006; Rowan et al., 2002; Śliwiński et al., 2016). If the carbonate cements within this shale bed formed at temperatures of 20-75°C (the approx. temperature range from the sediment-water interface in a tropical seaway to the approx. temperature above which bacterial activity in sediments declines decisively; *e.g.,* Heese, 1999), then the measured range of cement $\delta^{13}C$ values (+3 to +15‰; Figs. 3B, 6D) is consistent with cement formation from ^{13}C-enriched precursor CO_2.

Within the sandstone beds of the upper Mt. Simon Fm., $\delta^{13}C$ values of dolomite-ankerite cement zones 0 through 4 fall between -3 and +1‰, and are generally consistent with seawater as the dominant source of dissolved inorganic carbon for early carbonate cement formation. The more negative $\delta^{13}C$ values of the latest ankerite cement zones 5 and 6, which fall between -5 and -9‰, suggest the involvement of two end-member processes in their formation: 1) contributions of isotopically light CO_2 derived from the breakdown and recycling of organic matter, or simply 2) the effect of burial-related heating on the extent of carbon-isotope fractionation between DIC in the pore-fluid and the precipitating carbonate phase. In the case of the first process, an external source of carbon (perhaps from deeper in the basin) would have likely been needed, as these arenitic sandstone beds were likely buried with only a minimal amount of organic matter. The second process, on the other hand, can readily account for the observed ~10‰ range in $\delta^{13}C$ values. For example, consider that lower Paleozoic strata of the Illinois Basin in central Illinois are modeled to have experienced transient heating to 150-200°C during mid-Permian time (*ca.* 270 Ma). This is thought to have occurred in association with cross-basin brine migrations events that resulted in the genesis of Mississippi-Valley type ore districts (Pb-Zn mineralization) on the basins' northern and southern margins (at *ca.* 270 Ma) (Rowan et al., 2002). For a constant CO_2 $\delta^{13}C$ value, a temperature range of 20-150°C would result in a range of ~10‰ in dolomite $\delta^{13}C$ values ($\delta^{13}C_{dolomite}$ values at 150°C would be 10‰ lower than at 20°C; a ~12‰ range would be observed if temperatures reached 200°C) (Horita, 2014).

References

Heese, R., 1999. Early diagenetic pore water/sediment interaction. Diagenesis, Geoscience Canada, Reprint Series 4, 277–316.

Horita, J., 2014. Oxygen and carbon isotope fractionation in the system dolomite–water–CO_2 to elevated temperatures. Geochimica et Cosmochimica Acta 129, 111–124. doi:10.1016/j.gca.2013.12.027

Irwin, H., Curtis, C., Coleman, M., 1977. Isotopic evidence for source of diagenetic carbonates formed during burial of organic-rich sediments.

Makowitz, A., Lander, R.H., Milliken, K.L., 2006. Diagenetic modeling to assess the relative timing of quartz cementation and brittle grain processes during compaction. AAPG Bulletin 90, 873–885. doi:10.1306/12190505044

Rowan, E.L., Goldhaber, M.B., Hatch, J.R., 2002. Regional fluid flow as a factor in the thermal history of the Illinois basin: Constraints from fluid inclusions and the maturity of Pennsylvanian coals. AAPG Bulletin 86, 257–277.

Śliwiński, M.G., Kozdon, R., Kitajima, K., Denny, A., Valley, J.W., 2016. Microanalysis of carbonate cement $\delta^{18}O$ in a CO_2-storage system seal: Insights into the diagenetic history of the Eau Claire Formation (Upper Cambrian), Illinois Basin. AAPG Bulletin 100, 1003–1031.

Whiticar, M.J., 1999. Carbon and hydrogen isotope systematics of bacterial formation and oxidation of methane. Chemical Geology 161, 291–314.